EXPERIMENTAL STUDY OF THE EFFECT OF INTERFACIAL GAPS ON THE IN-PLANE BEHAVIOUR OF MASONRY INFILLED RC FRAMES

by

Chuanjia Hu

Submitted in partial fulfilment of the requirements
for the degree of Master of Applied Science

at

Dalhousie University
Halifax, Nova Scotia
June 2015

To mom and dad

爱你们

TABLE OF CONTENTS

LIST OF TABLES

LIST OF FIGURES

ABSTRACT

Previous studies on masonry infilled frames have shown that gaps between the infill and the bounding frame can significantly affect the stiffness and strength of the infilled system. However, the relationship between the magnitude and location of the gap and the stiffness and strength of the infill has not been thoroughly studied. In addition, the majority of the existing research on gap effects has been focused on infilled steel frames with only a few studies on reinforced concrete (RC) frames. For design, the American standard MSJC 2011 states that the infill can be treated as a participating infill with a top gap of less than 9.5 mm, provided that the infill strength and stiffness are reduced by 50%. The Canadian standard CSA S304.1 does not allow any gaps for design of a participating infill. However, the validity of these provisions has not been thoroughly examined.

To investigate the effect of interfacial gaps on the in-plane behaviour and strength of masonry infills bounded by RC frames, five scaled masonry infilled RC frame specimens, as well as one bare RC frame specimen, were tested monotonically to failure under an in-plane lateral racking load. Parameters considered included gaps between the frame top beam and the infill, as well as between the frame columns and the infill. Two magnitudes, 7 and 12 mm, were studied for each gap situation. The load vs. lateral displacement response, failure mode, stiffness, strength, and ductility of each specimen were presented and discussed.

Experimental results showed that, when compared with the bare frame, the presence of infills significantly increased the initial stiffness and ultimate strength of the infilled frames regardless of the presence of gaps. When compared with the infilled frame with no gaps, the infilled frames with gaps showed a decrease in initial stiffness regardless of the gap location. Gaps of 7 mm did not cause significant reduction in ultimate load, whereas gaps of 12 mm resulted in a more pronounced reduction. It was found that unreinforced masonry bounded by RC frames had improved ductility when compared to unreinforced masonry alone. The ductility of the masonry infilled frames was comparable to that of the RC bare frame.

For the stiffness prediction, CSA S304.1 grossly overestimated the stiffness of the infilled frame without gaps. Reducing the calculated strut width by 60% resulted in a better stiffness estimate for the infilled frame without gaps. The MSJC design stiffness agreed reasonably well with the experimental stiffness. For the strength prediction, both CSA S304.1 and MSJC 2011 provided reasonable and conservative estimates of the ultimate strength for the infilled frames with no gaps. For the gapped specimens, the reduction on both the stiffness and strength due to gap effects was proposed.

LIST OF ABBREVIATIONS AND SYMBOLS USED

ABBREVIATIONS

BF	Bare Frame
CC	Corner crushing
CMUs	Concrete masonry units
COV	Coefficient of variation
DC	Diagonal cracking
IFNG	Infilled frame with no gaps
IFTG	Infilled frame with a top gap
IFSG	Infilled frame with side gaps
LVDT	Linear variable differential transformer
RC	Reinforced concrete
SS	Shear sliding

SYMBOLS

A_{nv}	Net shear area
A_w	Horizontal cross-sectional area of the infill wall
A_{uc}	The uncracked portion of the effective cross-sectional area providing shear bond
b_w	Actual thickness of the web of the infill
d	Diagonal length of the infill

d_v	Actual depth of a masonry wall in direction of shear considered
e	Eccentricity of the load
E_f, E_m	Elastic modulus of the frame, infill
f_{bs}	Bond shear strength of the infill
f'_c	Concrete compressive strength
f'_m	Compressive strength of the masonry
f'_{m-0}	Masonry strength parallel to bed joins
f'_{m-90}	Masonry strength perpendicular to bed joins
f_y	Steel yield strength
f_y	Steel ultimate strength
F_u	Ultimate collapse load of infilled RC frames
h, h'	Height of the infill, frame
H_{CC}	Corner crushing strength of the infill
H_{DC}	Diagonal cracking strength of the infill
H_{SS}	Shear sliding strength of the infill
H_u	Ultimate load of the infilled frame
I_b	Moment of inertia of the beam
I_c	Moment of inertia of the column
K_{cra}	Crack stiffness
K_{CC}	An empirical constant for corner crushing with a mean value of 246 mm
K_{DC}	An empirical constant for diagonal cracking with a mean value of 0.066
K_{ini}	Initial stiffness

K_{ult}	Ultimate stiffness
l	Length of the infill
l'	The beam span
M_f	Factored moment at the section considered
M_p	Least of plastic moment capacity of the beam and columns
M_{pb}	Plastic moment capacity of the beam
M_{pc}	Plastic moment capacity of the column
M_{pj}	Least of the beam, column, and their connection plastic moment capacity
M_y	Yield moment capacity of the section considered
N_u	Factored compressive force
P_1	Minimum compressive force acting normal to the sliding plane taken as P_d
P_d	Axial compressive load on the section considered
P_{d1}, P_{d2}, P_{d3}	The load at the drift of 1%, 2% and 2.5%
P_{cra}	Crack strength
P_r	Factored axial load resistance
P_{ult}	Ultimate strength
P_w	Vertical load acting on the infill
R	Ductility factor
t	Thickness of the infill
t_e	Effective thickness of the infill
t_f	Thickness of the flange of the concrete masonry unit
V_f	Factored shear at the section considered

V_n	Nominal shear strength
V_r	Ultimate shear load of different failure modes
w	Width of the diagonal strut
θ	Angle whose tangent is the infill height-to-length aspect ratio, in radians.
μ	Coefficient of friction on the interface between the frame and infill
α_b	Contact length of the infill and the beam
α_c	Contact length of the infill and the column
α_h, α_l	Vertical, horizontal contact length of the frame and the diagonal strut
α_r	Aspect ratio of the infill
λ	Non-dimensional relative stiffness parameter
γ_g	Factor to account for partially grouted and ungrouted walls constructed of units
τ_m	Shear strength of mortar
σ_c	Crushing strength of the infill
v_m	Shear strength of masonry
ϕ_m	Resistance factor for masonry
Δ_u, Δ_y	Ultimate, yield displacements
χ	Factor to account for direction of compressive stress in a masonry member relative

ACKNOWLEDGEMENTS

Let me start by first thanking my supervisor, Dr. Yi Liu, for her support and guidance during my studies at Dalhousie University. This dissertation would not have been possible without her irreplaceable contribution.

I would like to thank Canadian Concrete Masonry Products Association for providing the financial assistance, and Wildwood Masonry Ltd and Masonry Industry Association of Atlantic Canada for providing the labour and materials.

I would like to thank Dr. John Newhook and Dr. Andrew Corkum, my committee members, for taking the time to review this thesis and providing valuable feedback.

I would like to thank my fellow colleagues, Xiaoyan Zeng and Ehsan Nasiri, for their helpful collaboration on completing the experiments.

I would like to thank Mr. Blair Nickerson, Mr. Brian Kennedy, Mr. Brian Liekens, and Mr. Jesse Keane, for their kind assistance during the experimental portion of this research. I also would like to thank Daniel Buiza, Xi Chen, Riccardo Ciccarelli, and Vahid Farajkhah, for their kind help in casting the concrete frames.

Finally I would like to thank my family, especially my parents, for their endless love, belief, and support.

CHAPTER 1 INTRODUCTION

1.1 BACKGROUD

Masonry has commonly been used in frame building structures as infill walls as shown in Figure 1.1. They fulfill the function of either partitions to separate spaces or claddings to complete the building envelope. Although they have inherently large stiffness and strength, masonry infills are often treated as non-structural elements in practice. The lateral and gravity loads are designed to be resisted by the bounding frame only. However, if masonry infills are built tight against the bounding frame, ignoring their contribution to the stiffness and strength of the infilled system will not necessarily result in a safe and economical design. Instead, the presence of infills will attract large forces to the frame region and thus affects the lateral load distribution of the structure. If not designed properly, they may compromise the stability of the frame system. Hence, an accurate evaluation of the infill contribution to the stiffness and strength of the infilled system is critical.

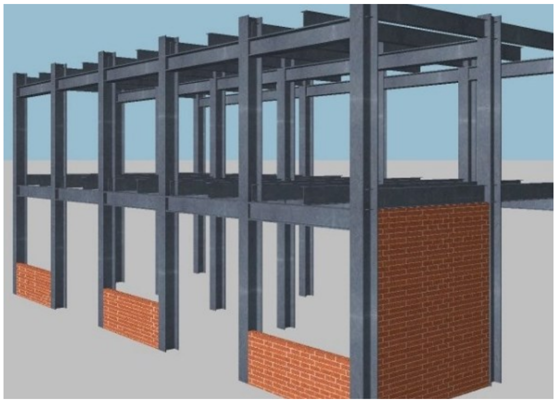

(a)

(b)

Figure 1.1 Applications of masonry infills

(a) Steel moment resisting frame with brick masonry partitions (world house encyclopedia); (b) Reinforced concrete frame with brick masonry infills (Charleson, A.)

The research on the behaviour of infilled frames dated back in 1960's. Since then, both experimental and numerical studies have been conducted to study the stiffness and strength of infilled frames with the majority of the experiments conducted around 1980's. These studies have showed the complexity of masonry infilled systems as they are affected by material and geometric properties of both the frame and the infill, the stiffness ratio of the frame and the infill, and loading conditions. It was found that largely scattered and even conflicting results were reported among the studies. In 2000's, with the development of computing technologies, studies have been more focused on the numerical modelling of the masonry infill using finite element methods. Although some analytical models have been proposed, experimental results with the current masonry products and construction are in need for the validation of these models. For design practice, the Canadian Masonry

Standard CSA S304.1 (2004) provides some guidelines for the design of masonry infill walls. But the method used is based on the study conducted 40 years ago (Stafford-Smith and Carter 1969) and only limited to simple and ideal cases. For example, CSA S304.1 requires that the masonry infill wall be built tight against the bounding frame, i.e., no gaps between the frame and the infill are allowed. However, the presence of interfacial gaps between the frame and the infill is not uncommon. The interfacial gaps commonly exist due to the shrinkage and settlement of the infill or defects in workmanship. On the other hand, the American Masonry Design Standard, MSJC 2011, states that the infill can be treated as a participating infill with a top gap of less than 9.5 mm with some form of strength and stiffness reduction for the infill. However, the background of the value of the reduction and the gap size limit is not clear. To provide a better understanding of masonry infilled RC frames with interfacial gaps and to examine the efficacy of the masonry codes and several analytical methods, an experimental program was carried out to investigate the effect of interfacial gaps on the in-plane behaviour and strength of masonry infills bounded by RC frames.

1.2 RESEARCH OBJECTIVES

This research involved experimental investigation of the in-plane behaviour and strength of masonry infills with a focus on the effect of the gap magnitude and location. The discussion was concentrated on the behaviour of the masonry infills.

A detailed description of the research objectives is as follows:

1. To provide a better understanding of the behaviour of masonry infilled RC frames with interfacial gaps.

2. To analyze the effect of interfacial gaps between the masonry infill and the bounding frame on the stiffness, strength, and ductility of the infilled frame.

3. To compare the experimental results from this research with the values calculated based on several existing analytical methods as well as the design provisions specified in CSA S304.1 and MSJC 2011.

1.3 DOCUMENT ORGANIZATION

The thesis consists of six chapters. Chapter 1 includes an introduction along with objectives and scope of this thesis. Chapter 2 presents a comprehensive literature review of various methods for the stiffness and strength calculations, North American masonry design codes, and previous studies involving interfacial gaps. Chapter 3 provides a detailed description of the experimental program, which included the construction of masonry infilled RC frames, test set-up, and auxiliary tests of the materials used. Chapter 4 contains a description and discussion of the results from the experimental program. Chapter 5 gives an evaluation of the design codes and several analytical methods by comparing the experimental results with the analytical values. Chapter 6 presents a summary of the research and the conclusions draw from this study.

CHAPTER 2 LITERATURE REVIEW

2.1 INTRODUCTION

The main task of this research is to investigate the effect of initial gaps between the infill and its bounding frame on the in-plane behaviour, stiffness, and strength of masonry infilled RC frames with a focus on the masonry infill. The following sections present a summary of general behaviour of infilled frames, current code practice in North America for design of infills, and previous studies conducted in the area of infilled frames with particular attention paid to the effect of interfacial gaps. The focus is kept on RC frames although results of tests on steel frames are also reported when deemed relevant.

2.2 GENERAL BEHAVOUR OF INFILLED FRAMES

A large number of studies have contributed to the development of the "equivalent diagonal strut method", a method that treats the entire infill as a single diagonal strut connecting loaded corners for the consideration of the infilled frame stiffness. It was observed in previous experiments that diagonal cracks developed in the central region of the infill, and as load increased, the bounding frame began to deform resulting in separation between the infill and the frame member. At failure, only the two loaded diagonal corners remained in full contact with the bounding frame, as shown in Figure 2.1.

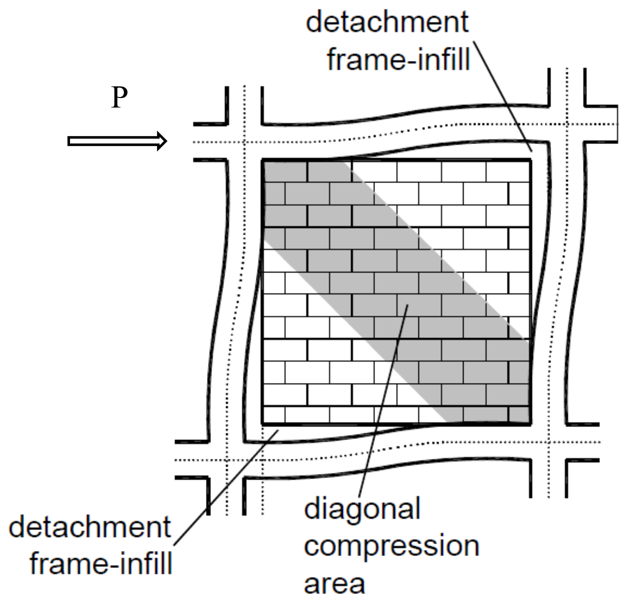

Figure 2.1 Equivalent diagonal strut model

(Adapted from Asteris et al. (2011))

Polyakov (1956) first proposed the diagonal strut method in the infilled frame analysis. In his in-plane loading test on a three-storey, three-bay infilled steel frame, the system behaved more as a diagonally braced frame with a compression strut based on the observation of cracking patterns. Stress transmission from the frame to the infill was only reported to occur in the compression area of the interface of the frame and the infill. The ends of the compression diagonal were where deformation concentrated whereas the ends of tension diagonals showed the separation of the infill from the frame.

2.2.1 Width of Equivalent Strut

Since the inception of the equivalent diagonal strut model, the research attention has been focused on the determination of the width of the diagonal strut that can be used to simulate the behaviour of the actual infill within a bounding frame. Once the strut width is known, assuming that the thickness and material properties of the strut are the same as the infill, a simple braced frame analysis can be performed to determine the infilled frame stiffness. Various formulae have been recommended for calculating the effective width of the diagonal strut. Generally, the proposed widths ranged from a simple percentage of the diagonal length of the infill to a function of the relative stiffness of the infill and the frame. It is noted that unless otherwise specified, the symbols used in this document are defined at their first appearance and are used consistently throughout.

In the category of the width as a percentage of the diagonal length of the infill, several important findings are noted as follows. Holmes (1961) recommended that the effective width of the equivalent strut can be taken as one-third (1/3) of the diagonal length of the infill by performing in-plane loading tests on single-bay infilled steel frames. Moghaddam and Dowling (1988) suggested that the width of the strut can be considered as one-sixth (1/6) of the diagonal length of the infill from experimental studies of scaled RC frames with brick infills. Stafford-Smith and Coull (1991) concluded that the effective width of the strut was one-tenth (1/10) of the infill diagonal length. Paulay and Priestley (1992) advised that one-quarter (1/4) of the diagonal strut length was a reasonable estimate of the strut width in infilled RC frames. Angel (1994) stated that the effective width of the strut can be calculated as one-eighth (1/8) of the diagonal length of the infill from experimental results of infilled RC frames. Despite the simplicity of these methods in application, the large variations of the different studies place their efficacy in question.

Stafford-Smith and Carter (1969) conducted a series of experiments on diagonally-loaded infilled steel frames and showed that the contact length between the infill and the column, α_c, was a function of the relative stiffness parameter of the infill to the frame, λ.

$$\frac{\alpha_c}{h'} = \frac{\pi}{2\lambda h'} \qquad [2.1]$$

and λ was based on the relative stiffness of the infill to the frame and the aspect ratio of the infill:

$$\lambda = \sqrt[4]{\frac{E_m t \sin 2\theta}{4 E_f I_c h}} \qquad [2.2]$$

where E_m and E_f are the moduli of elasticity of the masonry and frame, respectively; I_c is the moment of inertia of the column; θ is the angle whose tangent is the infill height-to-length aspect ratio in radians; t is the thickness of the infill; h is the height of the infill; h' is the height of the frame. With the contact length between the infill and the beam taken as half of the beam span, the width of the diagonal strut, w, was suggested as:

$$w = \sqrt{\alpha_c^2 + \left(\frac{l'}{2}\right)^2} \qquad [2.3]$$

where l' is the beam span.

The majority of the equations summarized subsequently adopted this relative stiffness parameter λ. Mainstone (1971) proposed two sets of equations to calculate the width of the diagonal strut based on a series of experiments conducted on small scale infilled steel frames.

(a) For brick infill

$$w/d = 0.175(\lambda h')^{-0.4} \quad 4 \le \lambda h' \le 5 \qquad [2.4]$$

$$w/d = 0.16(\lambda h')^{-0.3} \quad \lambda h' \ge 5 \qquad [2.5]$$

(b) For concrete infill

$$w/d = 0.115(\lambda h')^{-0.4} \quad 4 \le \lambda h' \le 5 \qquad [2.6]$$

$$w / d = 0.11(\lambda h')^{-0.3} \quad \lambda h' \geq 5 \qquad [2.7]$$

where d is the diagonal length of the infill panel.

Liauw and Kwan (1984) conducted finite element analysis which neglected the friction at the interface of the infill and frame. They suggested the use of the equation presented below to estimate the width of the diagonal strut.

$$w = \min\left(\frac{0.86 h \cos\theta}{\sqrt{\lambda h}}, 0.45 h \cos\theta\right) \qquad [2.8]$$

Al-Chaar (2002) presented the following equations to calculate the width of the diagonal strut in masonry infilled frames of both RC and steel frames. For l/h between 1.0 and 1.5, linear interpolation can be used.

$$w = 0.0835 B d\left(1 + \frac{2.574}{\lambda h'}\right) \text{ for } \frac{l}{h} \geq 1.5 \qquad [2.9]$$

$$w = 0.1106 d\left(1 + \frac{6.027}{\lambda h'}\right) \text{ for } \frac{l}{h} = 1.0 \qquad [2.10]$$

where,

$$B = -0.3905\frac{l}{h} + 1.7829 \qquad [2.11]$$

where l is the length of the infill.

El-Dakhakhni et al. (2003) showed that using a single diagonal strut was inadequate to accurately simulate the bending moment and shearing forces in the frame members. They believed that a three-strut model can better represent the real force distribution of the infill and frame. Figure 2.2 shows the idealization of their model. The total strut area can be determined by multiplying the width calculated using Equation [2.12] by the thickness of the infill.

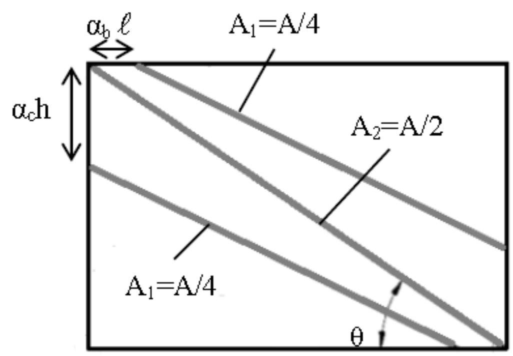

Figure 2.2 Three-strut infilled frame model

(Adapted from EI-Dakhakni et al. 2003)

$$w = \frac{(1-\alpha_c)\alpha_c h}{\cos\theta} \qquad [2.12]$$

where,

$$\alpha_c h = \sqrt{\frac{2(M_{pj} + 0.2M_{pc})}{tf'_{m\text{-}o}}} \leq 0.4h \qquad [2.13]$$

where M_{pj} is the plastic moment capacity of the joint, taken as the least of plastic moment capacity of the beam, the column, and the connection; M_{pc} is the plastic moment capacity of the column; $f'_{m\text{-}0}$ is the masonry strength parallel to bed joints. $\alpha_b l$ in the figure is given as:

$$\alpha_b l = \sqrt{\frac{2(M_{pj} + 0.2M_{pb})}{tf'_{m\text{-}90}}} \leq 0.4l \qquad [2.14]$$

where $f'_{m\text{-}90}$ is the masonry strength perpendicular to bed joints.

2.2.2 Failure Modes of Infilled Frames

Different failure modes of infilled frames have been reported for either infilled RC or steel frames (Rosenblueth 1980; Liauw and Kwan 1983; Angel 1994; Mehrabi et al. 1996; Galanti et al. 1998; El-Dakhakhni 2002; Drysdale and Hamid 2005; Liu and Soon 2012). Five failure modes as presented in the following have been identified.

(a) The compression strut out-of-plane buckling mode, as displayed in Figure 2.3, happens due to a slender infill, where crushing is observed in the central region of the infill.

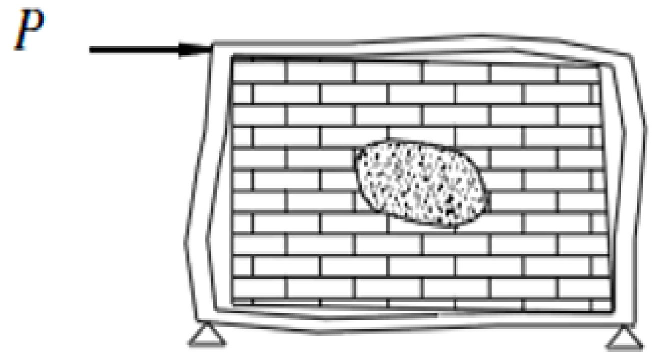

Figure 2.3 Compression strut out-of-plane buckling mode

(Adapted from El-Dakhakhni 2002)

(b) The shear sliding mode, representing horizontal sliding along a bed joint or the bottom side of the masonry infill, as displayed in Figure 2.4, commonly occurs in a case with an infill of weak mortar joints and a strong frame.

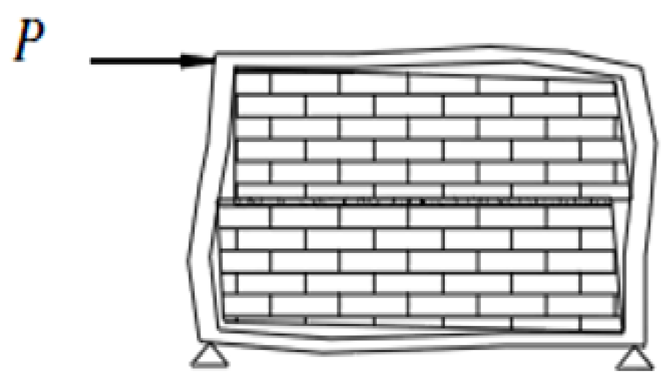

Figure 2.4 Shear sliding mode

(Adapted from El-Dakhakhni 2002)

(c) The diagonal cracking mode, seen in the form of cracks along the compressed diagonal, as displayed in Figure 2.5, is usually associated with an infill of strong mortar joints.

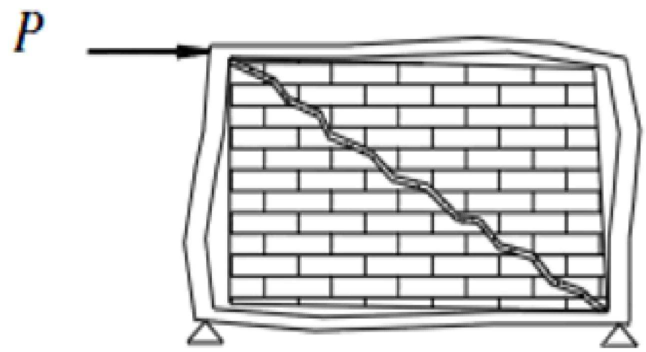

Figure 2.5 Diagonal cracking mode

(Adapted from El-Dakhakhni 2002)

(d) The corner crushing mode, representing crushing of the infill observed at the loaded corners, as displayed in Figure 2.6, is commonly associated with a weak masonry infill confined by a relatively strong frame.

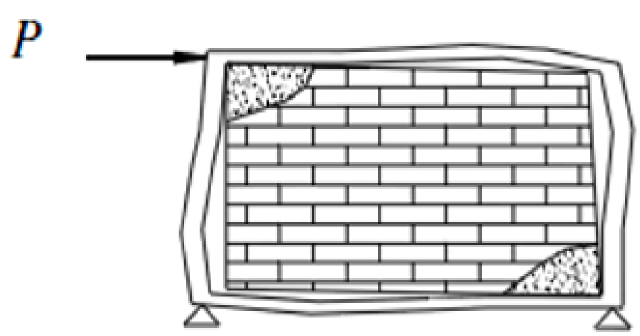

Figure 2.6 Corner crushing mode

(Adapted from El-Dakhakhni 2002)

(e) The frame failure mode, characterized by plastic hinges developing at the columns or the beam-column connections, as displayed in Figure 2.7, is usually seen in a case with a weak bounding frame.

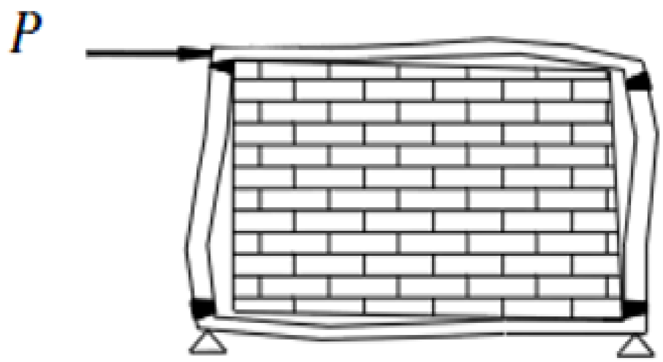

Figure 2.7 Frame failure mode

(Adapted from El-Dakhakhni 2002)

Of all the aforementioned failure modes, corner crushing and shear sliding modes have occurred more frequently in previous experimental studies. But for infills of typical geometry and material properties encountered in practice, corner crushing is more predominant and thus has more importance (Comité Euro-International du Béton CEB, 1996). The compression strut out-of-plane buckling mode occurred rarely and might only be a concern for the infill of a high slenderness ratio. Although the diagonal cracking mode is also commonly seen (Soon 2011; Manesh 2013), it should not be treated as a final failure since the infill can still sustain additional loads after cracking. As for the frame failure mode, although it might occur in weak RC frames, this mode hardly happens in steel frames (El-Dakhakhni et al. 2003).

2.2.3 Strength of Infilled RC Frames

This section reviews the studies of infilled RC frames with attention paid to the strength calculation. The strength is dependent on the failure mode of infilled frames which in turn depends on the geometric and material properties of the infilled system.

Mainstone (1971) proposed the following equation to calculate the corner crushing load, H_{CC}, of brick infills based on the equivalent strut method. λ is the relative stiffness parameter of the infill to the frame, as defined in Equation [2.2].

$$H_{CC} = 0.56(\lambda h')^{-0.875} f'_m \, h' t \cot\theta \qquad [2.15]$$

where f'_m is the compressive strength of the masonry infill.

Wood (1978) developed an equation for the calculation of the ultimate collapse load of an infilled RC frame considering shear capacity of both the frame and infill.

$$F_u = \frac{4M_p}{h} + \frac{1}{2}\sigma_c lt \qquad [2.16]$$

where F_u is the ultimate collapse load; M_p is the smaller plastic moment of the beam and columns; and σ_c is the crushing strength of the infill.

Rosenblueth (1980) reported two equations to estimate the capacity of infill panels bounded by RC frames for shear sliding and corner crushing failure. The force of the shear sliding failure, H_{SS}, was a function of the aspect ratio and shear strength of the mortar while the force of the corner crushing failure, H_{CC}, was dictated by the strut width and compressive strength of the masonry.

$$H_{SS} = \left(0.9 + 0.3\frac{l}{h}\right) f_{bs} ht \qquad [2.17]$$

$$H_{CC} = \frac{2}{3}\alpha_c t f'_m \sec\theta \qquad [2.18]$$

where α_c is the contact length of the infill and column, as defined in Equation [2.19]; f_{bs} is the bond shear strength of the masonry infill.

$$\alpha_c = \frac{\pi}{2}\sqrt[4]{\frac{4E_f I_c h}{E_m t_e \sin 2\theta}} \qquad [2.19]$$

Liauw and Kwan (1983) described two typical failure modes, i.e. corner crushing and diagonal crushing mode with different failure positions, of fully integrated infilled frames using a plastic analysis method. Equation [2.20] refers to corner crushing with failure in columns and infill-beam connections; Equation [2.21] refers to corner crushing with failure in beams and infill-column connections; Equation [2.22] refers to diagonal crushing with failure in infill-beam connections; and Equation [2.23] refers to diagonal crushing with failure in infill-column connections.

$$H_u = \sigma_c t h' \sqrt{\frac{2(M_{pj} + M_{pb})}{\sigma_c t h'^2}} \qquad [2.20]$$

$$H_u = \frac{\sigma_c t h'}{\tan\theta} \sqrt{\frac{2(M_{pj} + M_{pb})}{\sigma_c t h'^2}} \qquad [2.21]$$

$$H_u = \frac{4M_{pj}}{h'} + \frac{\sigma_c t h'}{6} \qquad [2.22]$$

$$H_u = \frac{4M_{pj}}{h'} + \frac{\sigma_c t h'}{6\tan\theta} \qquad [2.23]$$

where H_u is the ultimate horizontal shear resistance of the infilled system; σ_c is the crushing strength of the infill; M_{pj} is the joint plastic moment capacity; M_{pb} is the beam plastic moment capacity.

Stafford-Smith and Coull (1991) proposed the following equation to determine the corner crushing load of the infill.

$$H_{CC} = f'_m t \frac{\pi}{2} \sqrt[4]{\frac{4E_f I h'}{E_m t}} \qquad [2.24]$$

Mehrabi et al. (1996) assessed the effect of vertical loading on the lateral resistance of an infilled RC frame based on the shear sliding mechanism. Based on the Mohr-Coulomb criterion, the following equation was proposed, in which the two constants, i.e. 0.345 and 0.9, were the testing cohesive stress and the coefficient of friction, respectively.

$$H_{SS} = 0.345A_w + 0.9P_w \quad [2.25]$$

where H_{ss} is the horizontal shear of shear sliding failure; A_w is the horizontal cross-sectional area of the infill; P_w is the vertical load acting on the infill.

Galanti et al. (1998) observed two failure modes of masonry infilled RC frames, i.e. corner crushing and shear sliding failure. Equation [2.26] gives the strength of the infill of corner crushing failure, H_{CC}. However, the authors did not provide formula to calculate the strut width.

$$H_{CC} = f'_m\, wt\sqrt{1+\alpha_r^{\,2}} \quad [2.26]$$

The maximum sliding shear, H_{SS}, of the infill was primarily a function of the shear strength of the mortar as shown in Equation [2.27].

$$H_{SS} = \tau_m lt \quad [2.27]$$

where a_r is the aspect ratio of the infill; τ_m is the shear strength of the mortar.

Flanagan and Bennett (1999) presented two empirical equations for the strength calculation of clay tile infills based on the diagonal cracking and corner crushing failure, as shown in Equation [2.28] and [2.29], respectively.

$$H_{DC} = K_{DC} lt \sqrt{f'_m} \quad [2.28]$$

$$H_{CC} = K_{CC} tf'_m \quad [2.29]$$

where H_{DC} is the diagonal cracking strength; K_{DC} is an empirical constant for diagonal cracking with a mean value of 0.066; H_{CC} is the corner crushing strength; K_{CC} is an empirical value for corner crushing with a mean value of 246 mm.

Al-Chaar et al. (2002) conducted in-plane monotonic deflection-controlled pushover tests on five RC frames with concrete masonry infills to a horizontal displacement of 127~152 mm (approximately a 9% drift ratio). It was found that the infilled RC frames exhibited significantly higher peak and residual strength and initial stiffness than the bare frame. While maintaining high ductility, the infilled RC frames showed an increase in the peak strength and initial stiffness as the number of bays increased.

2.3 CODE PRACTICE IN NORTH AMERICA

2.3.1 CSA S304.1

The in-plane stiffness of masonry infilled frames in the Canadian Masonry Standard CSA S304.1 is determined based on the equivalent diagonal strut approach. The following equation is provided to determine the width of the diagonal strut based on the work done by Stafford-Smith and Carter (1969), which was later modified by Hendry (1981). The standard states that the effective strut width for the compressive capacity calculation shall be taken as $w/2$ and shall not be greater than one-fourth of the diagonal length.

$$w = \sqrt{\alpha_h^2 + \alpha_L^2} \qquad [2.30]$$

where α_h and α_L are the vertical and horizontal contact length of the frame and the diagonal strut, respectively. They both depend on the relative stiffness of the beams, columns, and masonry infill, as determined by the following equations:

$$\alpha_h = \frac{\pi}{2}\sqrt[4]{\frac{4E_f I_c h}{E_m t_e \sin 2\theta}} \qquad [2.31]$$

$$\alpha_L = \pi\sqrt[4]{\frac{4E_f I_b l}{E_m t_e \sin 2\theta}} \qquad [2.32]$$

where t_e is the effective thickness of the infill wall.

Figure 2.8 illustrates the geometric properties of the equivalent diagonal strut model adopted in CSA 304.1.

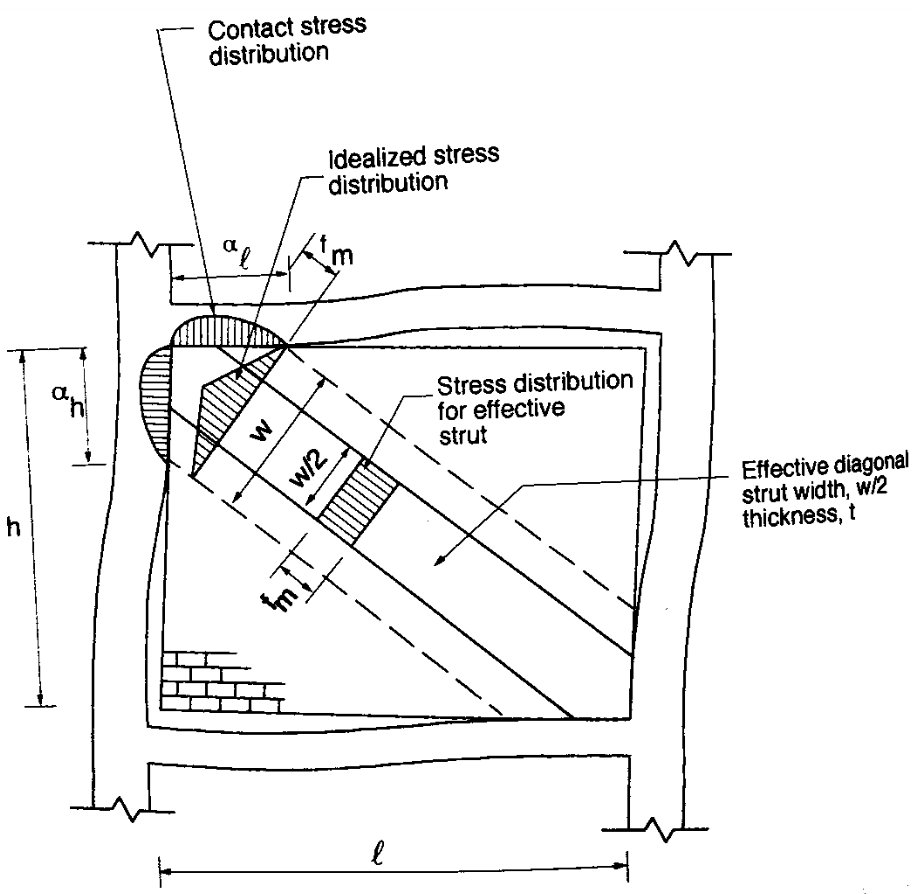

Figure 2.8 Illustration of geometric properties of the equivalent diagonal strut

(Adapted from Drysdale and Hamid 2005)

The in-plane strength of masonry infills in CSA S304.1 is determined with respect to three failure modes, i.e., corner crushing, shear sliding, and diagonal cracking. The details of the design procedures are presented in Chapter 5. As discussed earlier, corner crushing is considered to be the predominant failure mode and its ultimate capacity is calculated as the compressive capacity of the diagonal strut taking into account of the slenderness effect.

2.3.2 MSJC 2011

The American Masonry Standard MSJC 2011 also adopts the diagonal strut approach but provides a different equation to calculate the width of the diagonal strut based on the work of Flanagan and Bennet (1999):

$$w = \frac{0.3}{\lambda \cos\theta} \qquad [2.33]$$

where λ is the relative stiffness parameter as defined in Equation [2.2], but t in that equation is replaced by the effective thickness, t_e; θ is the angle whose tangent is the infill height-to-length aspect ratio in radians.

Similar to CSA S304.1, the infill strength in MSJC 2011 is also evaluated based on three failure modes while slightly different failure modes are defined. They are corner crushing, shear sliding, and 25 mm lateral displacement of the infilled frame. Details of the strength calculation procedures are presented in Chapter 5. For the predominant corner crushing failure mode, instead of using *w* obtained from Equation [2.33], MSJC 2011 simply uses a constant term of 6 inches as the diagonal strut width to account for the compressive capacity of the strut. The lateral strength of the infill is expressed as:

$$V_r = (6.0\text{in.})\, t_e f'_m \qquad [2.34]$$

It is worth noting that both the two codes use the effective thickness, t_e, of the infill instead of the total thickness, t, adopted in the previous studies. In accordance with CSA S304.1 and MSJC 2011, the effective thickness for hollow sections that are ungrouted or partially grouted is limited to the face shell thickness of the masonry units, whereas for hollow sections that are fully grouted it is the gross cross section thickness of the masonry units that takes the grout area into account.

2.4 STUDIES OF INTERFACIAL GAPS

Previous studies have shown that interfacial gaps between the infill and the bounding frame can significantly affect the stiffness and strength of the infill and hence the infilled system. For design, MSJC 2011 permits the use of infills as participating infills with a top gap of less than 9.5 mm but the stiffness and strength need to be reduced by 50%. It is, however, not clear whether this also applies to the case of side gaps. On the other hand, CSA S304.1

does not allow any gaps between the masonry infill and the bounding frame for design of a participating infill. The validity of these provisions concerning interfacial gaps has not been thoroughly examined. The following provides a review of the most relevant research involving initial gaps between frames and masonry infills.

Abdul-Kadir (1974) tested two small scaled brick infilled steel frames with a 1.6 mm gap between the infill and the beam. The tests showed no evident separation between the frame and the infill along the columns. The first shear crack appeared at the top courses of both the two walls under a low load, as shown in Figure 2.9. Prior to the failure, the wall behaved as a normal cracked wall in an infilled frame without gaps but had wider cracks. The failure was by corner crushing and the ultimate load was the same as that of the infilled frame with no gaps.

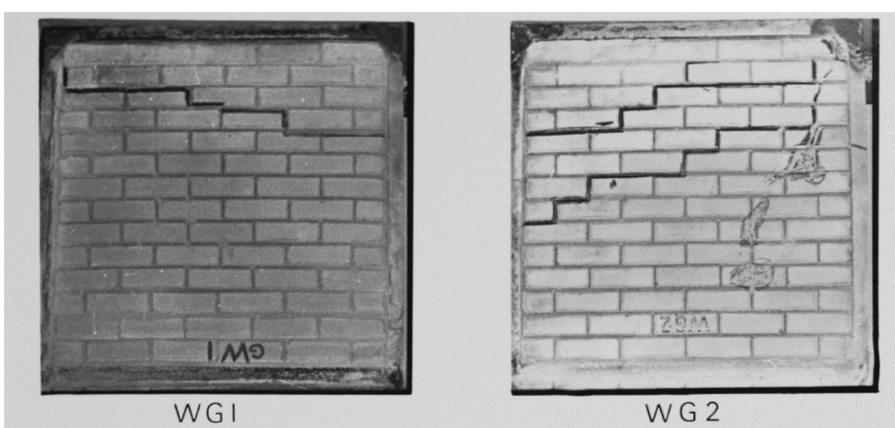

Figure 2.9 Failure mode of the infilled frames with a top gap

(Adapted from Abdul-Kadir 1974)

Riddington (1984) performed full-scale tests on concrete block infilled steel frames to study the effect of a 3 mm top gap and a 3 mm top gap plus 1.5 mm side gaps. For stiff frames, compared with the infilled frame with no gaps, the infilled frame with only a top gap showed an approximate 50% reduction in the stiffness and 7% decrease in the peak load; the infilled frame with both top and side gaps showed approximate 70% reduction in the stiffness and 15% decrease in the peak load.

Yong (1984) tested a steel frame with a concrete block masonry infill having a 10 mm gap between the upper edge of the infill and the roof beam. His study indicated that the specimen continued to gain strength once the gap closed at the loaded corner as if the gap had not existed.

Dawe and Seah (1989) studied the effect of the interface conditions between the top frame beam and the infill. They noted a slight reduction in the strength and stiffness when a bond breaker (a polyethylene membrane) was adopted at the top interface. They also noted that a top gap of 20 mm which was 0.8% of the height of the infill caused detrimental effects to the cracking pattern and ultimate capacity of the infilled frame system. A result of an approximate 50% decrease in the stiffness and a 60% reduction in the strength was observed.

Seah (1998) investigated a 25 mm gap between the infill panel and the roof beam in a numerical study. Analytical results showed that the infill panel had rotated and the top of the panel had contacted with the roof beam at a lateral deflection of 20 mm. When contact was made, an abrupt growth in the stiffness was observed and the system behaviour was to some extent similar to that of a fully bounded infill-frame system.

Flanagan and Bennett (1999) tested one clay tile infilled steel frame with a 25 mm gap between the infill and the column. They found that the gapped specimen was much softer than the specimen without gaps in the early stages of loading; but the stiffness was significantly larger than that of the bare frame.

Ng'andu (2006) tested calcium silicate element wall infilled steel frames which were monotonically loaded by in-plane loading. He investigated a 12 mm gap between the roof beam and the wall panel as shown in Figure 2.10 (a). The results showed that the gap caused a noticeable reduction (20%) in the infilled frame stiffness during the early stage of loading yet no significant decrease in the cracking load of the infill wall. In order to eliminate the negative influence of the top gap, the author investigated a novel construction technique of using bearing wedges at the top corner as shown in Figure 2.10 (b). The purpose of this technique was to improve the contact between the wall and the frame at the corners. The results showed that the infilled frame with corner bearing wedges and a top gap presented higher stiffness compared to the infilled frame without any gaps. However the author failed to identify the cause of this phenomenon but recommended further research in this area.

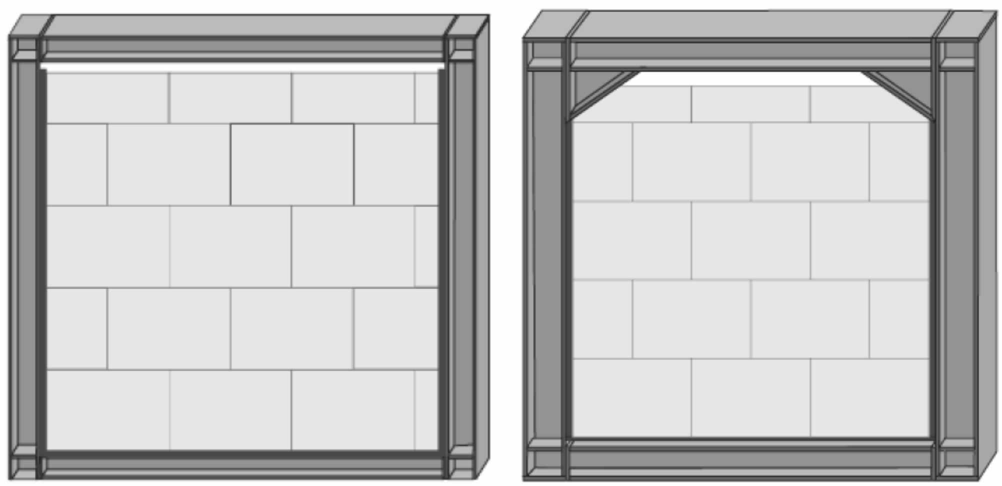

(a) (b)

Figure 2.10 (a) Specimen with a top gap;
(b) Specimen with a top gap and corner wedges

(Adapted from Ng'andu 2006)

Nazief (2014) investigated masonry infilled steel and RC frames having a full separation gap between the frame and the infill, as well as a top gap between the frame beam and the infill using finite element analysis. The sizes of the gaps considered were 5, 7, 10, and 15 mm. He concluded that the presence of a top gap did not have significant effect on the ultimate load of the infilled frames. For the full gap situation, according to the author, the contribution of the infill lateral resistance should be discounted when the gap is 10 mm; a full separation gap of up to 5 mm did not impact the in-plane behaviour of the infilled frames. The detailed reductions of the stiffness and strength for different gap situations from his study were presented in Table 2.1. It should be noted that the reductions were averaged for the gaps of 5 and 7 mm, as well as for the gaps of 10 and 15 m. Also included in this table are the aforementioned previous studies on the gap effects that had reported reductions of the stiffness and strength.

Table 2.1 Summary of previous studies on gap effects

Reference	Frame	Gap	Stiffness	Strength
Riddington (1984)	steel	a 3 mm top	-50%	-7%
		a 3 mm top + two 1.5 mm side gaps	-70%	-15%
Dawe and Seah (1989)	steel	a 20 mm top gap	-50%	-60%
Ng'andu (2006)	steel	a 12 mm top gap	-20%	little
Nazief (2014)	steel	a top gap of 5,7 mm	-27%	-9%
		a top gap of 10, 15 mm	-41%	-24%
		full gaps of 5,7 mm	-37%	-15%
		full gaps of 10, 15 mm	-71%	-50%
	RC	a top gap of 5,7 mm	-1%	-12%
		a top gap of 10, 15 mm	-5%	-19%
		full gaps of 5,7 mm	-64%	-31%
		full gaps of 10, 15 mm	-90%	-58%

Other researchers (Soon 2011, Manesh 2013) although did not investigate the effect of initial gaps between the infill and the surrounding frame in particular, they all recognized the undesirable influence of gaps on the stiffness and strength of infilled frames and adopted applicable methods such as filling up the gap with cement and shims to reduce the gap to a minimum value in their studies.

2.5 CONCLUDING REMARK

A large number of studies have been conducted to investigate the behaviour of infilled RC/steel frames, and various equations and analytical models have been proposed to account for the stiffness and strength of infill walls. Among those models, the single diagonal strut model is the most popular one and has been widely adopted because of its simplicity and acceptable accuracy within the elastic range. A variety of formulae have been reported for the determination of the strut width. Compared with the existing studies on other parameters, there is not enough technical information on the effect of initial gaps between frames and infills on the lateral stiffness and strength of the infilled frame. Despite that the presence of interfacial gaps has been reported to significantly affect the strength and stiffness, and sometimes even alter the failure mode of the infilled frame, the relationship between the magnitude and location of the gap and stiffness and strength of the infill has not been thoroughly studied. In addition, the majority of the existing research on the gap effects has been focused on infilled steel frames and results on RC bounding frames are limited.

CHAPTER 3 EXPERIMENTAL PROGRAM

3.1 GENERAL

The experimental program was designed to investigate the effect of interfacial gaps on the in-plane behaviour of concrete masonry infilled RC frames. A total of six scaled specimens were tested to failure under an in-plane lateral load applied at the centerline level of the frame top beam. Parameters considered included the location and magnitude of the interfacial gaps. Two gap locations, i.e., between the frame beam and the infill, and between the frame columns and the infill were considered. For each gap location, two magnitudes, 7 and 12 mm, were studied.

Concurrent with the testing of infilled frame specimens, auxiliary tests were performed to determine the material properties of concrete masonry units (CMUs), mortar, masonry prisms, concrete cylinders, and reinforcing steel. Detailed descriptions of the infilled frame specimens, test set-up, testing procedures, and auxiliary tests are presented in the following sections.

3.2 INFILLED FRAME SPECIMENS

Table 3.1 presents a summary of the frame specimens. The six specimens included one bare frame (BF) specimen without infill and five infilled specimens. The infilled specimens included one specimen with the infill built tight against the frame members and thus considered as the infilled frame with no gaps (IFNG). The remaining four infilled specimens included two specimens having gaps between the infill and the frame top beam (IFTG) and two specimens having gaps between the infill and the frame columns (IFSG).

Table 3.1 Summary of frame specimens

Number	Specimen ID	Gap
1	BF	N/A
2	IFNG	None
3	IFTG7	7 mm at top
4	IFTG12	12 mm at top
5	IFSG7	3.5 mm at each side
6	IFSG12	6 mm at each side

All the frame specimens had the same dimensions as shown in Figure 3.1. The required gap magnitudes were achieved by slightly adjusting the thickness of mortar. The geometry of the infill yielded a height-to-length aspect ratio of about 0.73. The infills were constructed using custom-made, half-scale standard 200 mm CMUs laying in the running bond. The infills were unreinforced and ungrouted. The efficacy of using scaled CMUs for infill walls has been validated by several researchers (Mehrabi et al. 1996, Mosalam et al. 1997, Maleki et al. 2007, Liu and Soon 2012). The nominal dimensions of the scaled CMUs are shown in Figure 3.2 for both stretchers and half blocks. The half blocks were obtained by cutting the stretcher blocks in half. All the dimensions in the figures below are in mm.

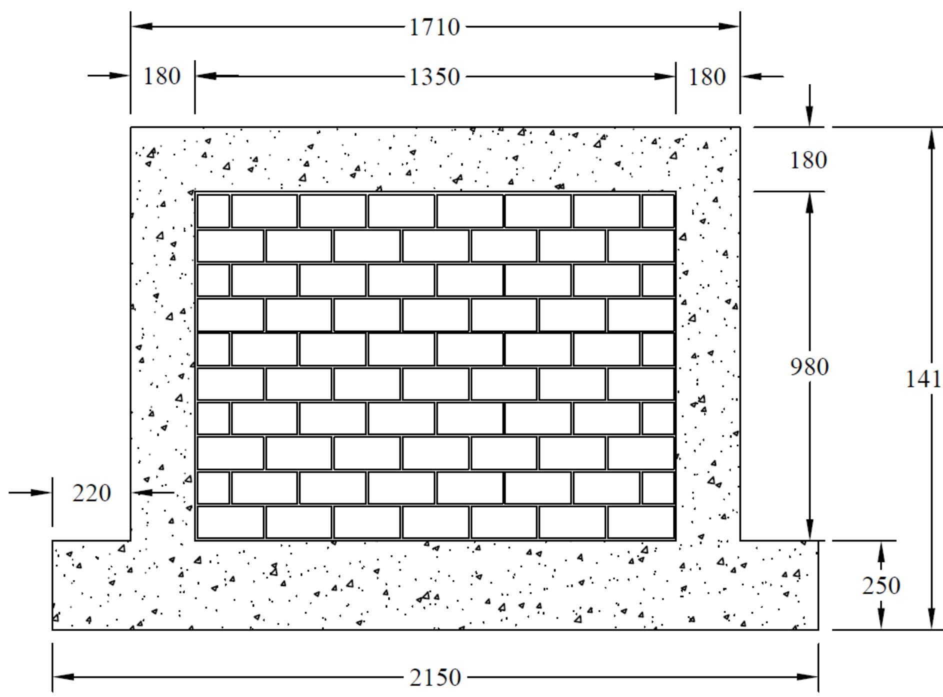

Figure 3.1 Geometric properties of infilled frame specimens

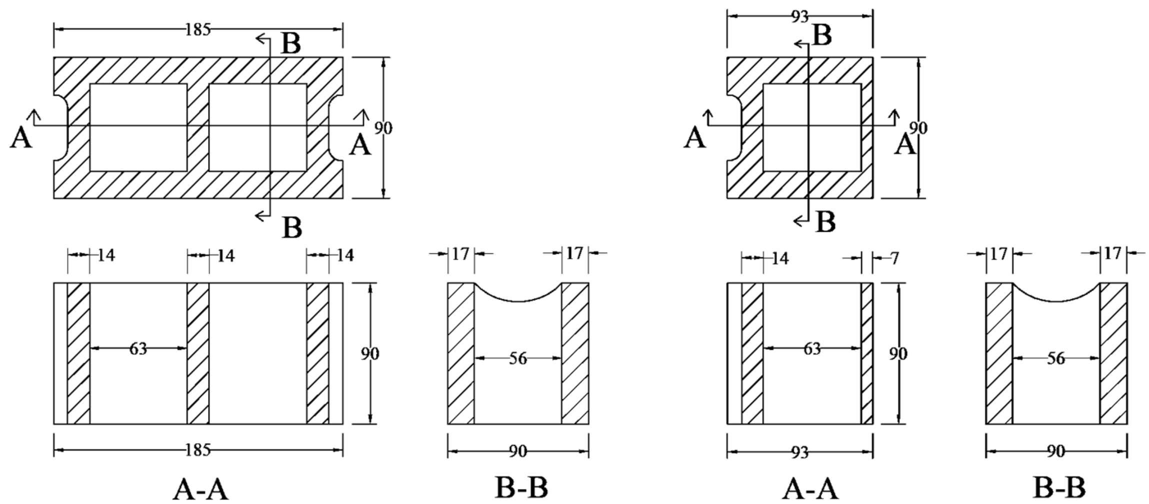

(a) Stretcher block (b) Half block

Figure 3.2 Details of half-scaled CMUs

The frame top beam and columns had a 180 mm square section reinforced with 4-10M deformed rebars and 10M stirrups spacing at 100 mm center-to-center. The base beam had a 250 mm square section reinforced with 4-15M longitudinal rebars and 10M stirrups spacing at 100 mm center-to-center. In addition, four 300×300 mm L-shaped 10M bars were used at each top beam-column corner for additional strengthening. The concrete cover used for the frame members was 25 mm. Details of the reinforcement are shown in Figure 3.3.

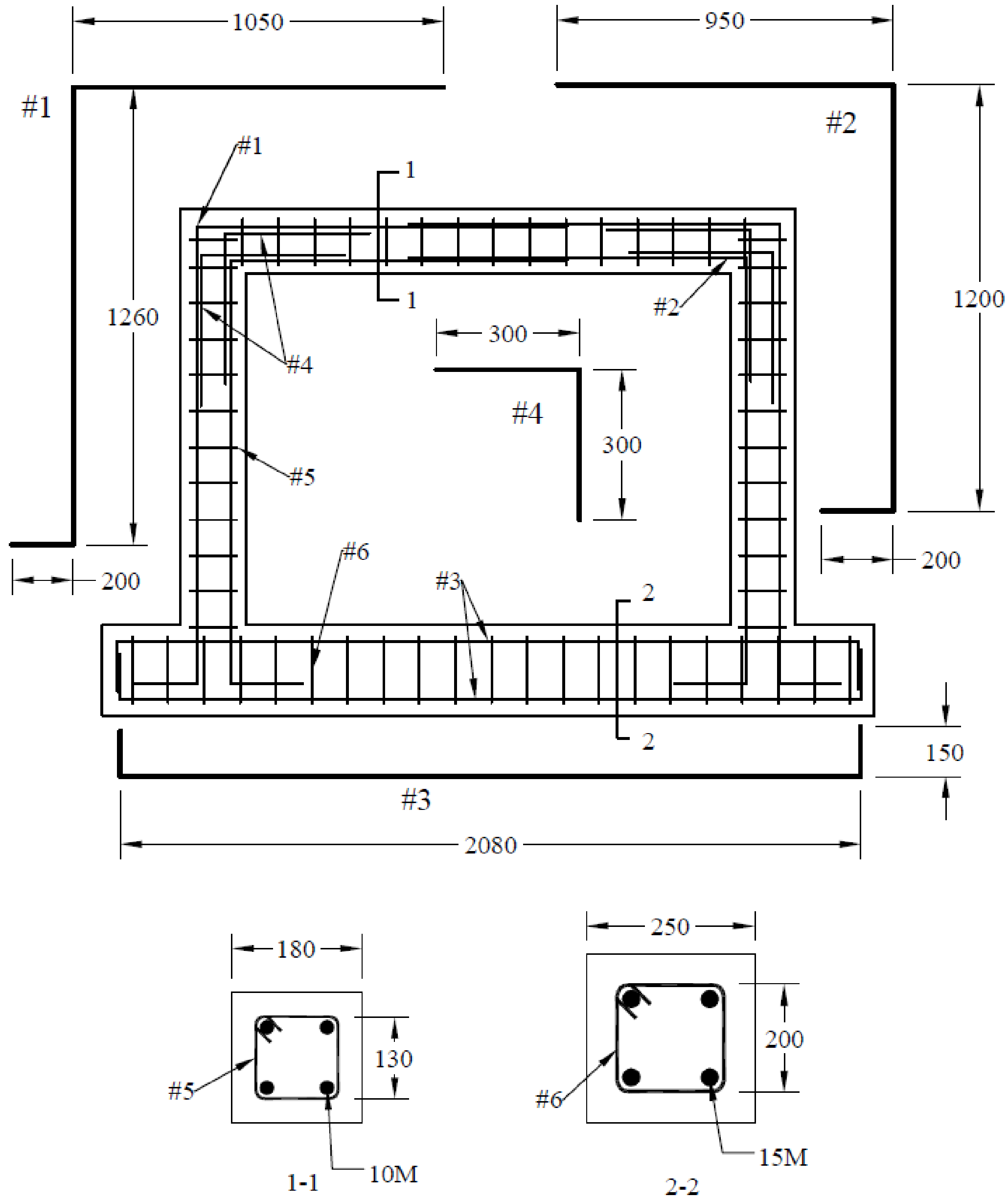

Figure 3.3 Details of reinforcement in RC frames

The rationale behind the design of the RC frame was to achieve that the frame fails shortly after the infill reaches its capacity. The equivalent diagonal strut of the infill and its capacity were first determined based on CSA S304.1. Then a braced frame analysis was conducted on S-FRAME to determine the load that can be applied on the infilled frame corresponding to the infill capacity. This load was used as the basis for the design of RC frame members. The calculation can be found in Appendix A. The final geometry and reinforcement of the frame sections were adjusted for construction considerations.

3.2.1 Construction of RC Frames

The construction of the RC frames consisted of fabricating formwork, placing and tying reinforcement steel in position, and casting concrete. Six sets of wood formwork were built for the RC frames. Figure 3.4 shows an overview of the formwork.

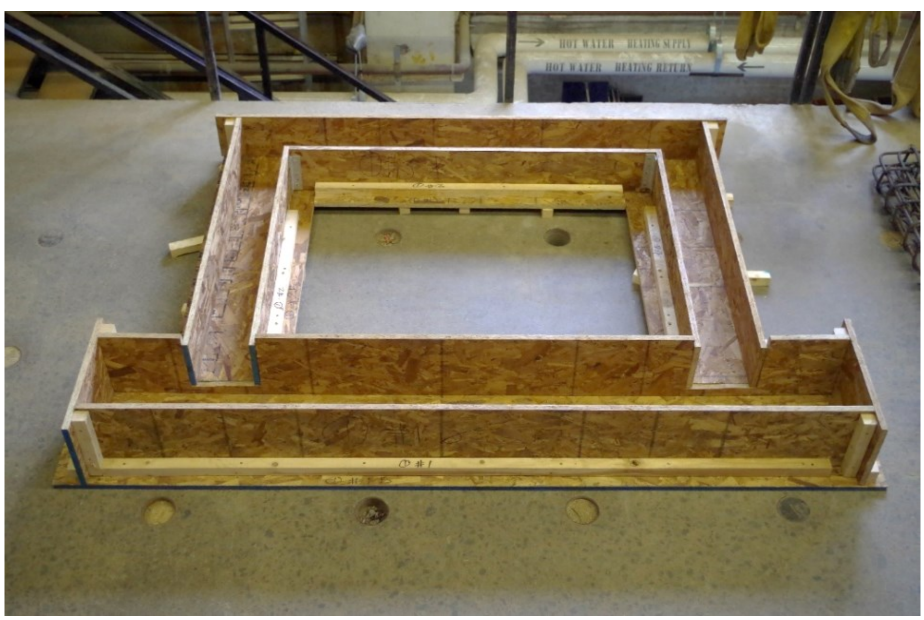

Figure 3.4 Overview of formwork

The concrete frames were cast in two batches. Specimen BF, IFNG, IFTG7, and IFTG12 were cast on July 16, 2014, whereas specimen IFSG7 and IFSG12 were cast on December 12, 2014. Prior to pouring concrete, the inner faces of the formwork were brushed with grease. After the reinforcement cage was properly positioned, U-shape clamps were placed to restrain horizontal expansion of concrete as shown in Figure 3.5. Plastic chairs with a height of 35 mm were used to ensure the needed concrete coverage as shown in Figure 3.6. The ready-mix concrete with a specified compressive strength of 35 MPa was used and a maximum coarse aggregate size of 12 mm was specified. When the concrete was transported to the laboratory, a slump test was conducted in accordance with ASTM C143/C143M (2012) Standard Test Method for Slump of Hydraulic-Cement Concrete. The slump test showed a falling height of 16 cm which satisfied the required 15 cm. The concrete was then poured into the formwork as quickly as possible and vibrated thoroughly with a concrete vibrator as shown in Figure 3.7. After the vibration, the concrete surface was smoothed over using concrete trowels. Figure 3.8 shows the completion of the concrete casting. The concrete cylinders were cast alongside the frame for the determination of concrete strength.

Figure 3.5 Overview of formwork with reinforcement

Figure 3.6 Details of formwork with reinforcement

Figure 3.7 Concrete casting and vibrating

Figure 3.8 Completion of concrete casting

3.2.2 Fabrication of Masonry Infill Walls

The masonry infill walls were built in two batches by an experienced mason to the standard of masonry construction practice. Specimen IFNG, IFTG7, and IFTG12 were constructed on August 26, 2014; specimen IFSG7 and IFSG12 were constructed on January 21, 2015. Figure 3.9 shows the various aspects of the masonry construction including cutting the blocks (a), marking the course lines on the concrete frame (b), construction process (c-e), and the final product (f). A level and plumb were used throughout the process to ensure the wall was straight and levelled. The mortar was applied on the block face shell only for both the bed joints and head joints. Two batches of mortar (A and B) were used to build the infill walls. The required gap magnitudes were achieved by slightly adjusting the thickness of the mortar. The masonry prisms and mortar cubes were constructed alongside the infill walls. All the wall specimens, masonry prisms, and mortar cubes were moist-cured under the same conditions for 28 days and then air-cured until the day of testing. The temperature variation in the laboratory ranged from 10°C to 25°C and the humidity varied from 60% to 80%.

(a) (b)

(c) (d)

(e) (f)

Figure 3.9 Construction of masonry infill walls

3.3 TEST SET-UP

A schematic view of the test set-up is illustrated in Figure 3.10 and a picture is shown in Figure 3.11. A hydraulic actuator with a capacity of 250 kN was used to apply the lateral load. The actuator was fastened to the column of the reaction frame using two 12 mm diameter bolts and a load cell was attached to the actuator to measure the load. A steel plate was placed between the load cell and the frame to ensure a uniform distribution of the concentrate load. The reaction frame consisted of a skewed A-frame including two W150×30 steel columns welded to a stiffened short W200×46 beam which was connected to the strong floor through high strength bolts. Two additional W150×30 columns were used to brace the reaction frame in the out-of-plane direction, as shown in Figure 3.12.

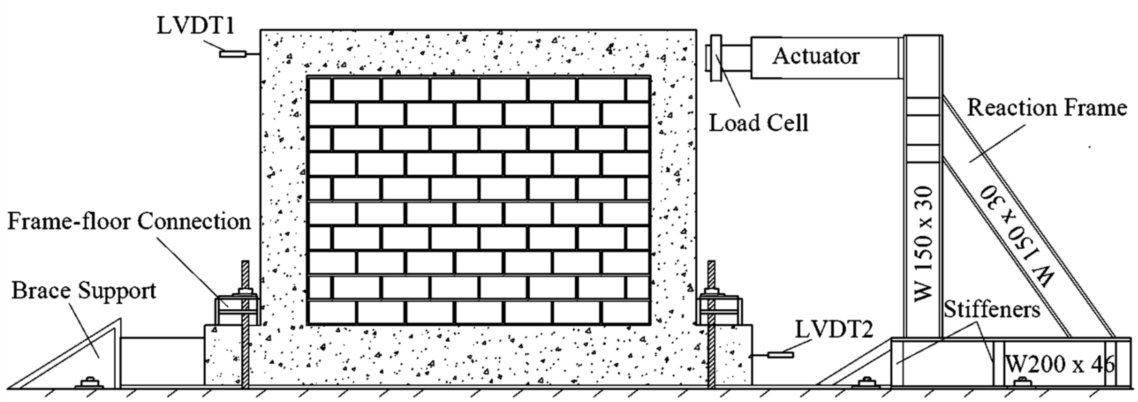

Figure 3.10 Schematic view of test set-up

Figure 3.11 Test set-up

Figure 3.12 Side view of the reaction frame

The frame base beam was clamped to the strong floor using two W-shape steel beams at its two side stems as shown in Figure 3.13.

Figure 3.13 Frame-to-floor connections

An additional brace support was used at one end of the frame stem to further restrain the in-plane sliding of the frame specimen as shown in Figure 3.14.

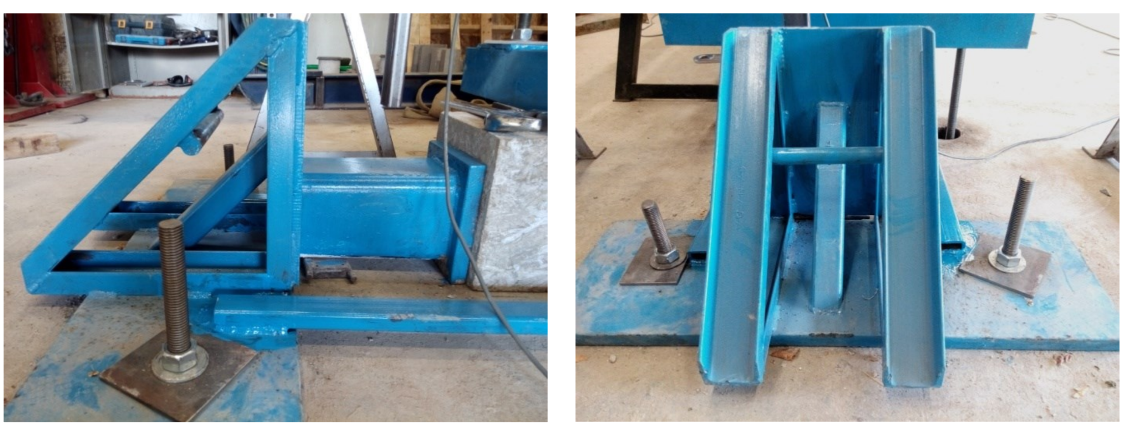

Figure 3.14 Brace support at far end

Two linear variable differential transformers (LVDTs) (LVDT 1 and 2) were mounted at the centerline of the top and bottom beam respectively to measure the in-plane lateral displacements as shown in Figure 3.15. LVDT 3 was positioned at the half height of the wall and LVDT 4 was positioned at the central point of the top beam, both on the back side, to monitor any possible out-of-plane movements of the infill wall and the concrete frame respectively, as shown in Figure 3.16.

Figure 3.15 Placement of LVDT 1 and 2

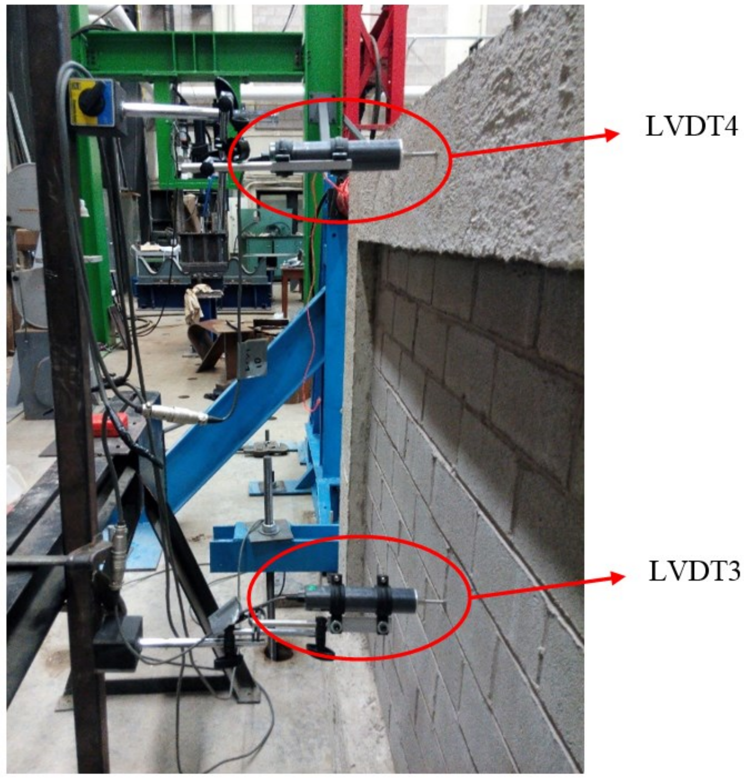

Figure 3.16 Placement of LVDT 3 and 4

3.4 TESTING PROCEDURES

Prior to the testing, the infilled frame specimen was positioned in place and was aligned carefully in both in-plane and out-of-plane directions. The load cell and all the LVDTs were then checked to ensure that they functioned properly. The lateral load was applied gradually at a rate of 6 kN per minute until the failure of the specimen. The load and LVDT readings were monitored and recorded with an interval of 0.2 seconds throughout the test using an electronic data acquisition system. For each test, the cracking load, ultimate load, cracking pattern, and failure mode were noted and photographed when necessary.

3.5 AUXILIARY TESTS

3.5.1 CMUs

The scaled CMUs were tested for the compressive strength according to ASTM C140/C140M (2014) Standard Test Methods for Sampling and Testing Concrete Masonry Units and Related Units as shown in Figure 3.17. Three blocks were selected randomly and placed in the Instron universal testing machine and capped with two pieces of fiberboard on the loading surfaces. The physical properties including 24-hour percentage absorption, density, and moisture content were tested in accordance with ASTM C140/C140M (2014).

Figure 3.17 Compression test set-up for CMUs

3.5.2 Mortar

Type S mortar was used in the masonry infill wall construction. Portland cement, type N masonry cement, and sand with a respective volume ratio of 1:3:12 were mixed thoroughly to make the type S mortar according to industry practice. Two batches (A and B) of mortar were mixed for the construction of the masonry infill walls and mortar cubes. A total of ten 50 mm mortar cubes were cast in a non-absorbent mould and cured in the same conditions as the masonry walls. The mortar cubes were tested in an Instron compression machine as shown in Figure 3.18 for their compressive strength on the day when the corresponding frame was tested. The sampling and testing of mortar cubes was performed in accordance with ASTM C270 (2014) Standard Specification for Mortar for Unit Masonry.

Figure 3.18 Compression test set-up for mortar cubes

3.5.3 Masonry Prisms

A total of ten 3-course high hollow masonry prisms were built and tested for the compressive strength in accordance with ASTM C1314 (2014) Standard Test Method for Compressive Strength of Masonry Prisms. The prisms were fabricated alongside the walls and cured in the same conditions. The mortar was applied on the face shell only. Similar to the testing of the concrete blocks, the prisms were placed in the Instron universal testing machine and capped with two pieces of fiberboard on the loading surfaces, as shown in Figure 3.19.

Figure 3.19 Compression test set-up for prisms

3.5.4 Concrete

The ready mix concrete with a specified compressive strength of 35 MPa was used for the RC frames. Two batches of concrete were used for the six frame specimens. Cylinder specimens S1~S6 were cast on July 16th, 2014, and S7~S12 were cast on December 12th, 2014. Three 100×200 mm and three 150×300 mm cylinders were made for each batch concrete. The small ones were tested at 7 days after the construction for quality control. The big ones were tested for the compressive strength and modulus of elasticity when the frame specimens were tested as shown in Figure 3.20. All the testing procedures were performed in accordance with ASTM C39/C39M (2014) Standard Test Method for Compressive Strength of Cylindrical Concrete Specimens.

Figure 3.20 Compression test set-up for concrete cylinders

3.5.5 Reinforcing Steel

Three steel coupons were randomly cut from 10M rebar stocks for the frame member reinforcement with details shown in Figure 3.21. They were tested in accordance with ASTM E8 (2008) Standard Test Methods for Tension Testing of Metallic Materials for their mechanical properties using Instron universal testing machine. The stress-strain relationship of the steel was obtained where the strain was measured using an extensometer as shown in Figure 3.22.

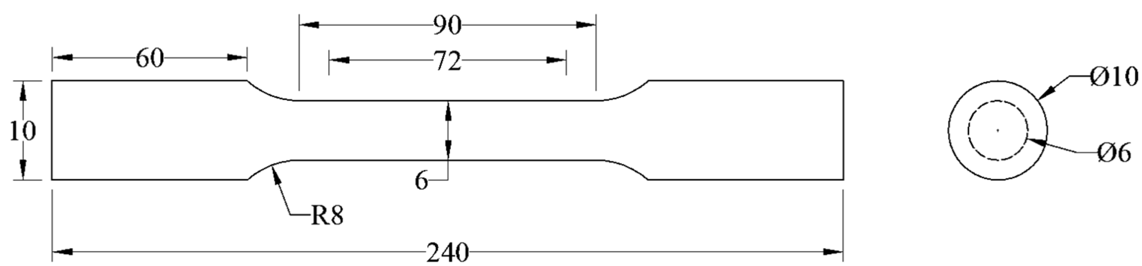

(a) Front view (b) Side view

Figure 3.21 Details of steel coupons

Figure 3.22 Tension test set-up for steel coupons

CHAPTER 4 RESULTS AND DISCUSSION

4.1 INTRODUCTION

This chapter presents the results of the auxiliary tests and infilled frame tests. The results of the auxiliary tests include physical and mechanical properties of the CMUs, mortar cubes, masonry prisms, concrete cylinders, and reinforcing steel. The results of the infilled frame tests are focused on the failure mode, stiffness, strength, and ductility of the infilled frames affected by the interfacial gaps of different magnitudes and locations.

4.2 RESULTS OF AUXILIARY TESTS

4.2.1 CMUs

The physical properties including net area, weight, absorption rate, moisture content, and density were obtained for the CMUs. Three randomly selected concrete blocks were used in the testing of these properties. Note that the custom-made blocks had recess in the webs hence only face shell areas were considered effective in transferring stress. The effective area was determined to be 6290 mm^2 on average. For the determination of absorption, moisture content, and density of the blocks, the procedures specified in ASTM

C140/C140M (2014) were followed. The received weight of each block was first measured and then the block was immersed in the water. The immersed weight was measured as the block was submerged in the water. After submerged for 24 hours, the block was removed from the water and towel dried. The weight of the block was measured at this point and this weight is termed as the saturated weight. The block was then dried in the oven at 100°C for 24 hours, after which the oven-dry weight was obtained. These weights were then used to calculate the block absorption, moisture content, and density. Table 4.1 presents the results with corresponding coefficient of variations (COV). The average absorption was 139.0 kg/m^3 with a COV of 4%. The average moisture content was 14.2% with a COV of 14% and the average density was 2118.6 kg/m^3 with a COV of 3%. According to CAN/CSA A165 (2004) Standards on Concrete Masonry Units, a standard 200 mm hollow block shall have an absorption of less than 175 kg/m^3, a density of greater than 2000 kg/m^3, and a maximum moisture content of 45% for a relative humidity higher than 75%. The averages of the results for the scaled CMUs demonstrated to be comparable with these specifications.

Table 4.1 Physical properties of CMUs

ID	Received Weight (g)	Immersed Weight (g)	Saturated Weight (g)	Dry Weight (g)	Absorption (kg/m^3)	Absorption (%)	Moisture Content (%)	Density (kg/m^3)
A1	1650.6	979.0	1736.5	1635.0	134.0	6.2	15.4	2158.4
A2	1631.3	967.7	1724.1	1618.9	139.1	6.5	11.8	2140.3
A3	1599.2	923.5	1692.6	1582.0	143.8	7.0	15.6	2057.0
				Avg.	139.0	6.6	14.2	2118.6
				COV	4%	6%	14%	3%

Table 4.2 summarized the mechanical properties of the CMUs. The average compressive strength was 22.0 MPa with a low COV of 5% based on an effective area of 6290 mm^2. This average compressive strength was shown to be comparable with the standard full scale CMUs with a compressive strength in the range of 10 to 40 MPa. Figure 4.1 shows a typical compressive failure mode of the CMUs, which features conical shear failure.

Table 4.2 Mechanical properties of CMUs

ID	Ultimate Load (kN)	Compressive Strength (MPa)
S1	141.5	22.5
S2	144.1	22.9
S3	130.3	20.7
	Avg.	22.0
	COV	5%

Figure 4.1 Typical compressive failure mode of CMUs (S1)

4.2.2 Mortar

Mortar batch A was used for the construction of specimens IFNG, IFTG7, and IFTG12, whereas mortar batch B was used for specimen IFSG7 and IFSG12. Table 4.3 presents the summary of the mortar cube dimensions and testing results. Mortar batch A showed a compressive strength of 21.0 MPa with a COV of 9%; mortar batch B showed a compressive strength of 21.5 MPa with a COV of 12%. The compressive strengths of the two batches were very close. The COVs were below the specified limit of 15% (CSA S304.1), which indicated that the mixture of mortar was consistent in the construction within each batch. Figure 4.2 shows a typical compressive failure mode of mortar cubes which showed a conical or pyramidal shape.

Figure 4.2 Typical compressive failure of mortar cubes (CA1)

Table 4.3 Compressive strength of mortar cubes

ID	Length (mm)	Width (mm)	Area (mm)	Ultimate Load (kN)	Compressive Strength (MPa)
Mortar Batch A (for IFNG, IFTG7 and IFTG12)					
CA1	49.0	50.5	2475	48.6	19.7
CA2	50.0	51.0	2550	49.2	19.3
CA3	50.0	50.5	2525	59.1	23.4
CA4	49.5	50.5	2500	56.5	22.6
CA5	49.5	50.5	2500	50.0	20.0
				Avg.	21.0
				COV	9%
Mortar Batch B (for IFSG7 and IFSG12)					
CB1	49.0	50.5	2475	48.3	19.5
CB2	50.0	51.0	2550	45.9	18.0
CB3	49.5	50.5	2500	59.1	23.6
CB4	49.5	50.5	2500	60.0	23.5
CB5	50.5	50.5	2550	57.2	22.9
				Avg.	21.5
				COV	12%

4.2.3 Masonry Prisms

For the calculation of the prism compressive strength, the effective cross sectional area, A_e, was used as shown in Figure 4.3 as the hatched area. The web was not included in the A_e calculation since mortar was only applied on the face shell. The average effective cross sectional area of the hollow prisms was 6290 mm^2. Table 4.4 lists the summary of the testing results. Prism batches A and B used mortar from mortar batches A and B, respectively. Prism batch A showed a compressive strength of 16.7 MPa with a COV of 10%; prism batch B showed a compressive strength of 17.1 MPa with a COV of 13%. The COVs of the two batches were well within the specified limit of 15%, indicating a consistent strength within each batch. Figure 4.4 shows a typical compressive failure mode of the prisms featuring tension cracks through either the face shell or the web.

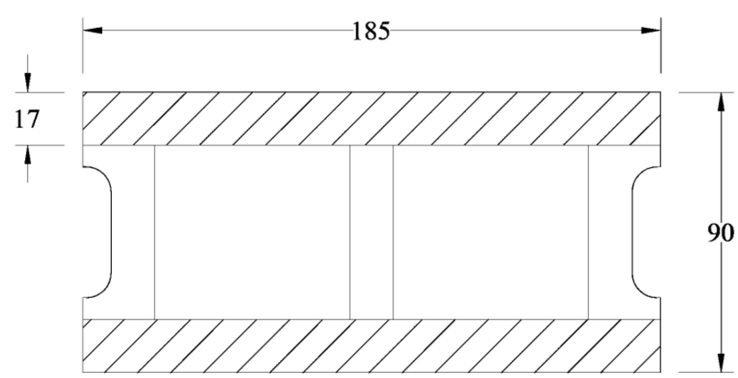

Figure 4.3 Effective cross sectional area of prisms

Table 4.4 Compressive strength of masonry prisms

Prism Batch A (for IFNG, IFTG7 and IFTG12)			Prism Batch B (for IFTG7 and IFSG12)		
ID	P_{ult} (kN)	f'_m (MPa)	ID	P_{ult} (kN)	f'_m (MPa)
PA1	97.4	15.5	PB1	100.0	15.9
PA2	100.4	16.0	PB2	128.9	20.5
PA3	111.3	17.7	PB3	117.5	18.7
PA4	112.8	17.9	PB4	94.8	15.1
PA5	103.7	16.5	PB5	95.6	15.2
	Avg.	16.7			17.1
	COV	10%			13%

Figure 4.4 Typical compressive failure mode of prisms (PA1)

4.2.4 Concrete

The concrete cylinders were tested for the compressive strength at the age of 7 days for quality control as well as at the date of the frame testing. The average cross-sectional areas of 100×200 mm and 150×300 mm concrete cylinders were 7850 mm^2 and 17663 mm^2, respectively. Concrete batch A was used in the construction of specimen BF, IFNG, IFTG7, and IFTG12, while batch B was used for specimen IFSG7 and IFSG12. For batch A, the average 7-day strength was 21.4 MPa with a COV of 9%; the average mature strength was 42.3 MPa with a COV of 3%, and the average modulus of elasticity was 28424 MPa with a COV of 4%. For batch B, the average 7-day strength was 23.0 MPa with a COV of 7%; the average mature strength was 45.3 MPa with a COV of 7%, and the average modulus of elasticity was 29295 MPa with a COV of 3%. The results showed that the concrete of the two batches was quite consistent. Table 4.5 lists the summary of the testing results. Figure 4.5 shows the initial stress vs. strain curve of the concrete cylinders under compression in the elastic range. Figure 4.6 shows a typical compressive failure mode of the concrete cylinders featuring a diagonal fracture with several vertical cracks.

Table 4.5 Compressive strength and elastic modulus of concrete cylinders

Concrete Batch A (for BF, IFNG, IFTG7 and IFTG12)						
7 Days	P_{ult} (kN)	f'_c (MPa)	58 Days	P_{ult} (kN)	f'_c (MPa)	E (MPa)
S1	184.75	23.5	S4	737.09	41.7	28798
S2	155.94	19.9	S5	770.35	43.6	29426
S3	162.39	20.7	S6	733.86	41.6	27047
	Avg.	21.4			42.3	28424
	COV	9%			3%	4%
Concrete Batch B (for IFSG7 and IFSG12)						
7 Days	P_{ult} (kN)	f'_c (MPa)	80 Days	P_{ult} (kN)	f'_c (MPa)	E (MPa)
S7	192.78	24.6	S10	836.75	47.4	29956
S8	167.83	21.4	S11	736.98	41.7	28361
S9	180.15	23.0	S12	825.10	46.7	29568
	Avg.	23.0			45.3	29295
	COV	7%			7%	3%

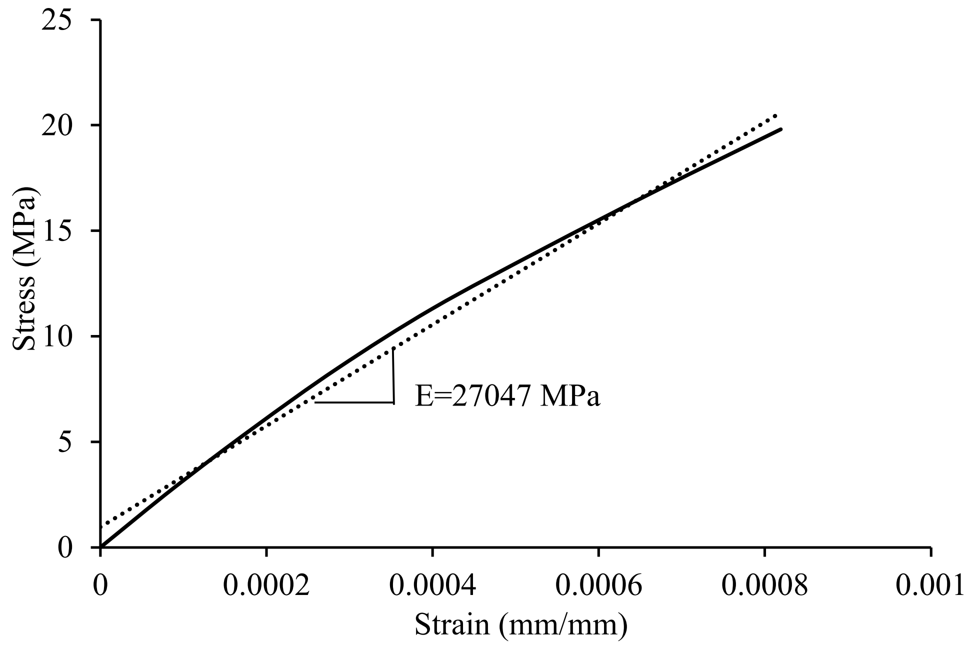

Figure 4.5 Initial stress vs. strain curve of cylinders under compression (S6)

Figure 4.6 Typical compressive failure mode of concrete cylinders (S4)

4.2.5 Reinforcing Steel

Three coupons were cut from the 10M longitudinal reinforcing steel and tested for their strength and modulus of elasticity. Figure 4.7 shows a typical tensile stress-strain curve of the steel coupons. As shown in Table 4.6, an average elastic modulus of 247,357 MPa, yield strength of 446 MPa, and ultimate strength of 665 MPa were obtained with low COVs. Figure 4.8 shows a flat surface of the failure plane of the coupon under tension.

Table 4.6 Properties of reinforcing steel

ID	E_s (MPa)	f_y (MPa)	f_u (MPa)
L1	249170	439	659
L2	245142	441	667
L3	247759	458	668
Avg.	247357	446	665
COV	1%	2%	1%

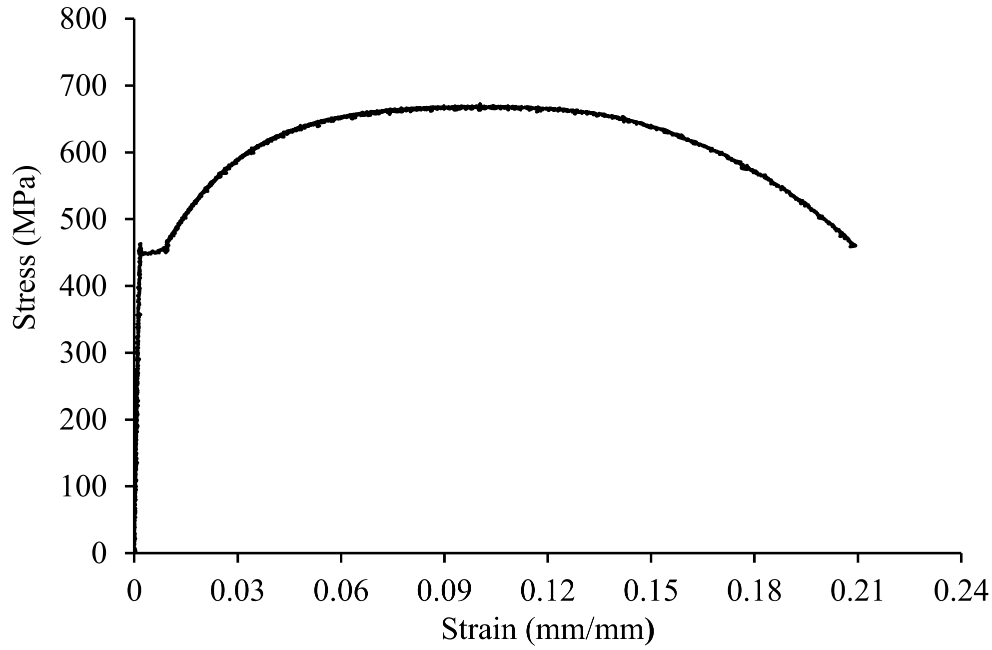

Figure 4.7 Typical tensile stress vs. strain curve of steel coupons (L3)

Figure 4.8 Failure of steel coupons under tension (L1)

4.2.6 Summary of Auxiliary Test Results

The results of the auxiliary tests are summarized in Table 4.7. Specimen BF, IFNG, IFTG7, and IFTG12 were built with materials of batch A; specimen IFSG7 and IFSG12 were built with materials of batch B. As shown in the table, the properties of these two batches were quite consistent.

Table 4.7 Summary of auxiliary test results

	Property	CMUs	Mortar	Prisms	Concrete	Reinforcement
Batch A	Strength (MPa)	22.0	21.0	16.7	42.3	446 (665)
	Elastic Modulus (MPa)	-	-	14195	28424	247357
Batch B	Strength (MPa)	22.0	21.5	17.1	45.3	446 (665)
	Elastic Modulus (MPa)	-	-	14535	29295	247357

4.3. SPECIMENS WITH A TOP INTERFACIAL GAP

4.3.1 General Behaviour

The load vs. lateral displacement responses of the infilled specimens without gaps or with a top gap were similar and their general behaviour can be divided into three stages. Figure 4.9 plots the load vs. lateral displacement curve of specimen IFNG as an example to illustrate this behaviour and define the terms used in this thesis.

The first stage covered the beginning of the loading to the load when the first major diagonal cracking occurred. Two stiffnesses, i.e., K_{ini} and K_{cra}, can be determined where K_{ini} was defined as the initial stiffness taken as the slope of the tangent line of the initial linear portion (up to 5% of the maximum load level) of the load vs. displacement curve whereas K_{cra} was defined as the crack stiffness taken as the slope of the line connecting the origin and the point having the first significant diagonal crack. In the first stage, when the load increased to about 20% of the ultimate load, small cracks began to form at the loaded corner of the concrete frame. At this point, the curve showed some deviations from the linearity indicating the stiffness reduction of the infilled system. At about 20 ~ 40% of the ultimate load, hairline cracks emerged along the diagonal direction in the infill while flexural cracks continued to develop through the height of the frame columns. At the end of the first stage, the hairline cracks in the infill developed into first major diagonal crack and the load vs. displacement curve showed a sudden drop. The second stage covered from the cracking load to the ultimate load where the system developed marked nonlinearity due to the development of diagonal cracking in the infill and flexural cracking in the frame columns. At the end of the second stage, the loaded corner of the infill crushed and the specimen reached its ultimate load. The slope of the line connecting the origin point and the peak load point was considered as the ultimate stiffness, K_{ult}. From the ultimate load to the stop of the test, the specimen entered the third stage still showing significant ductility when maintaining about 80% of the ultimate load while the cracking through the infill and crushing at the corner further developed. The remaining resistance was maintained in most cases while the specimens experienced large lateral displacement (>25mm). Also observed was the significant flexural cracking development in the RC frame columns.

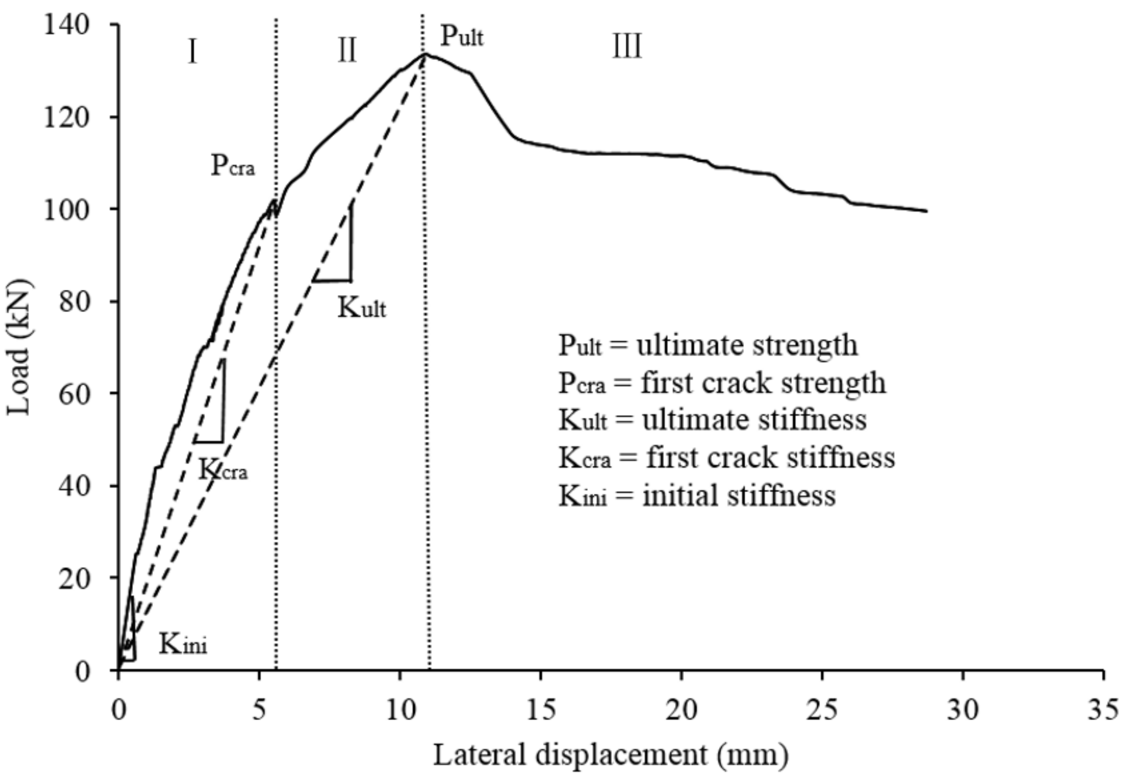

Figure 4.9 Load vs. lateral displacement curve of specimen IFNG

4.3.2 Failure Modes

Corner crushing was observed to be the final failure mode of the infilled frame specimen without gaps (IFNG) and those with a top gap (IFTG7 and IFTG12), as shown in Figure 4.10(c), 4.11(c), and 4.12(c). The failure was initiated by the cracking developed along the general diagonal direction of the infill. The general behaviour of these specimens was described in the previous section while the following noted the difference in failure modes where the effect of gaps was concerned.

Specimen IFNG and IFTG7 experienced evident separation of the infill from the column at the unloaded corner at the load of about 50 kN and 40 kN respectively, as shown in Figure 10(b) and 11(b). Specimen IFTG12 did not show visible separation as shown in Figure 12(b). The frame top beam and the infill remained in contact throughout the test for specimen IFNG as shown in Figure 10(c). The 7 mm top gap of specimen IFTG7 was closed at the loaded corner at about 80% of the ultimate load as shown Figure 11(c) while specimen IFTG12 still had a visible gap along the top beam after failure as shown in Figure 12(c). Additionally, as shown in Figure 10(a), 11(a), and 12(a), the presence of the top gap affected the diagonal cracking extent. Specimens IFNG and IFTG7 sustained one major diagonal crack while specimen IFTG12 experienced more extensive diagonal cracking. It suggests the cracking extent of the infill increased as the top gap size increased.

(a) Overview

(b) Left upper corner

(c) Right upper corner

Figure 4.10 Failure pattern of specimen IFNG

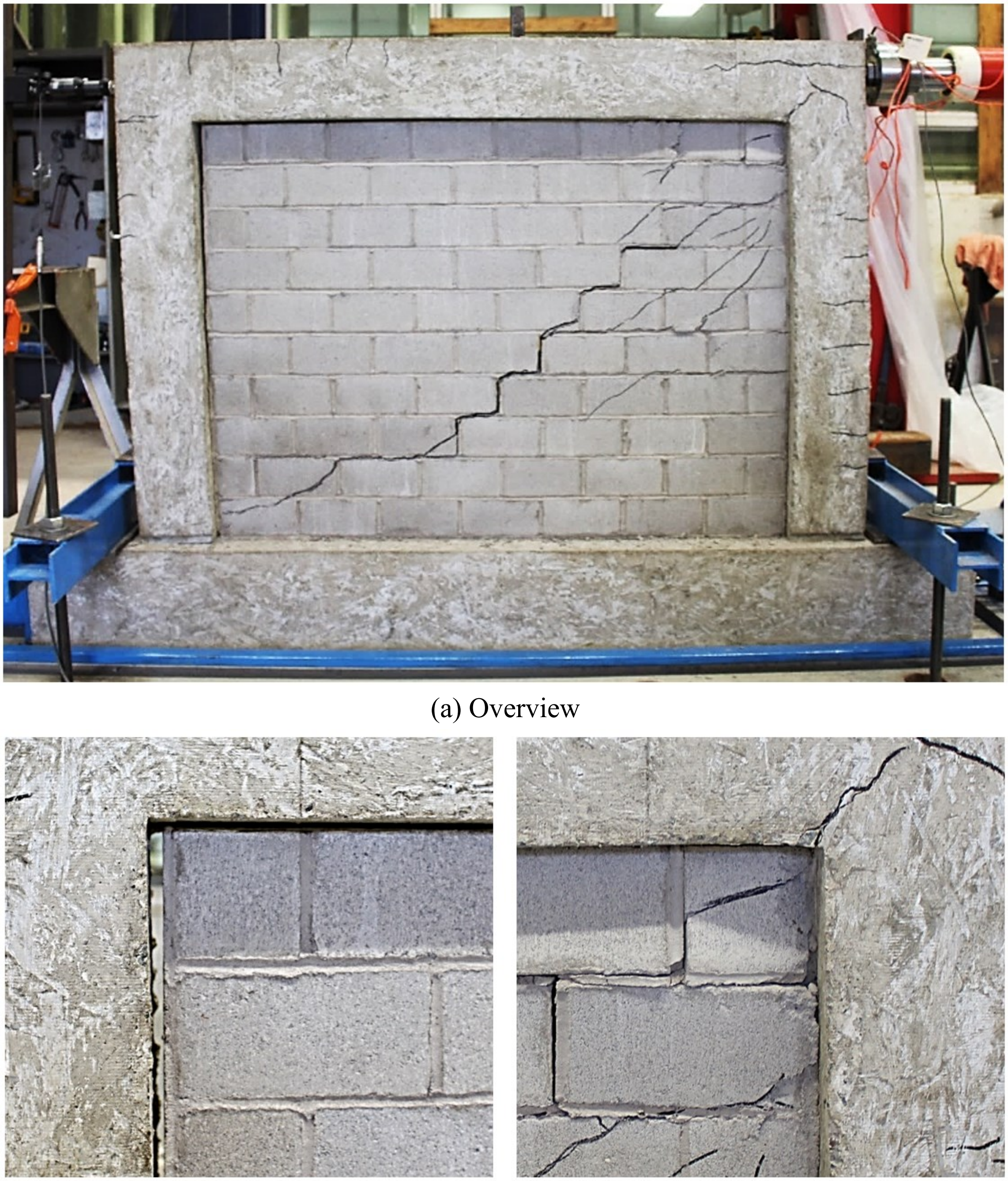

(a) Overview

(b) Left upper corner

(b) Right upper corner

Figure 4.11 Failure pattern of specimen IFTG7

(a) Overview

(a) Left upper corner (b) Right upper corner

Figure 4.12 Failure pattern of specimen IFTG12

4.4 SPECIMENS WITH SIDE INTERFACIAL GAPS

4.4.1 General Behaviour

The load vs. lateral displacement responses of the infilled specimens with side gaps were also obtained and their general behaviour can be divided into four stages. Figure 4.13 plots the load vs. lateral displacement curve of specimen IFSG7 as an example to illustrate the behaviour.

At the first stage, the specimen with side gaps behaved more or less as the bare frame with a slightly higher stiffness. This additional stiffness is likely due to the resistance provided by the interfacial friction between the infill and frame top beam. As the load continued to increase and the lateral displacement increased to close the initial side gap at the loaded side, the specimen began to enter the second stage showing an increase in the stiffness as the infill began to contribute to the system stiffness. At the end of the second stage, a shear sliding along a bed joint occurred which was reflected as a sudden drop on the load vs. lateral displacement curve. As the sliding developed through the bed joint and the occurrence of small cracks in the infill and the frame, the system showed noticeable nonlinearity, which was defined as the third stage. After reaching the ultimate load, the specimen was in the fourth stage featuring marked ductility. In this stage, the specimen was still capable of sustaining the load with significant deformation accompanied by the development of shear sliding along the bed joints and crushing in the infill corner at the loaded point. Also observed was the significant flexural cracks developed in the RC frame columns. The definition of the initial stiffness, crack stiffness, ultimate stiffness, first crack strength, and ultimate strength followed the same logic as the specimens with a top gap.

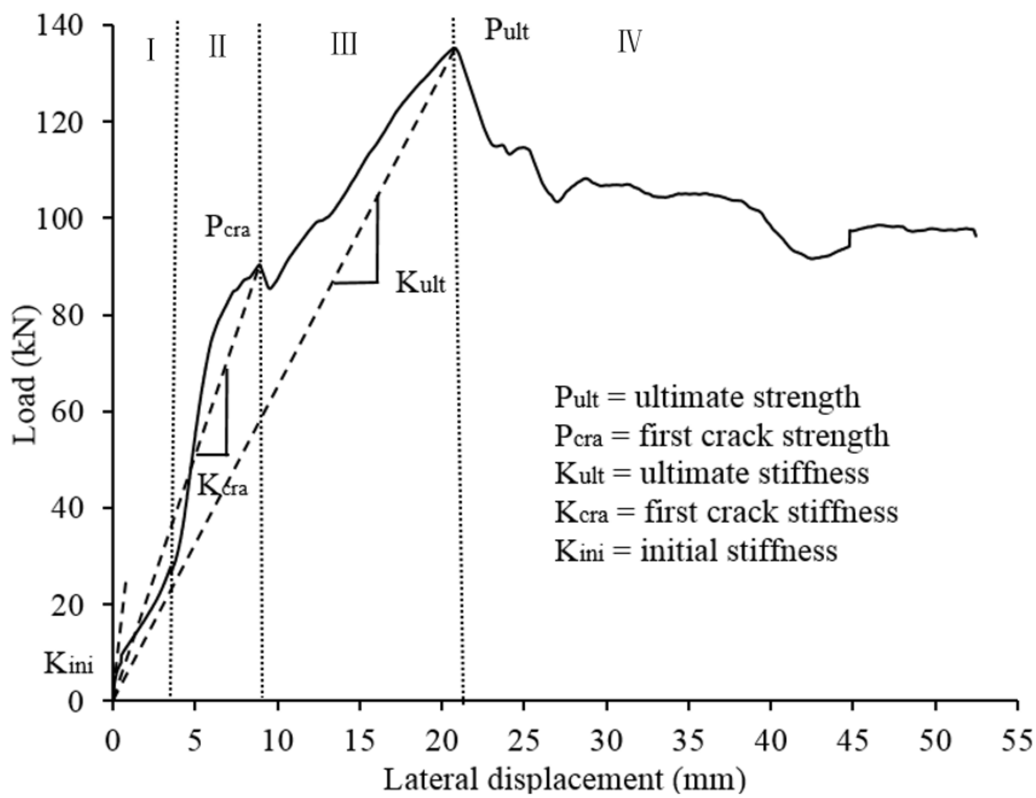

Figure 4.13 Load vs. lateral displacement curve of specimen IFSG7

4.4.2 Failure Modes

Corner crushing was also observed to be the final failure mode of the specimens with side gaps, as shown in Figure 4.14(c) for specimen IFSG7 and in Figure 4.15(c) for specimen IFSG12. The difference between these two specimens and those with a top gap was that the final failure was initiated by shear sliding along the bed joints.

In the case of specimen IFSG7, the contact of the column and the infill at the loaded side was made at the load of about 26 kN. Shear sliding was first observed at the load of about 90 kN at the first layer bed joint from the top beam, as shown in Figure 4.14(a) and 4.14(b). As the load increased to about 100 kN, shear sliding was also developed along the bottom layer of mortar (Figure 4.14(d)) and the infill was pushed against the lower part of the frame column at the unloaded side (Figure 4.14(e)). As the load continued to increase to failure, the crushing of the infill was observed at the loaded corner and at which point, the load began to decrease. It was noticed that there was no evident diagonal cracking for this specimen.

In the case of specimen IFSG12, the contact of the column and the infill at the loaded side was made at the load of about 33 kN. Shear sliding was first observed at the fifth layer bed joint as shown in Figure 4.15(a) at the load of about 65 kN. As the load increased to about

70 kN, shear sliding also developed throughout the bottom layer of mortar, as shown in Figure 4.15(e) and the infill portion between two sliding plane was pushed against the lower part of the frame column at the unloaded side. The loaded corner crushed at failure. It should be noted that a diagonal crack also occurred almost simultaneously as the crushing of the infill corner.

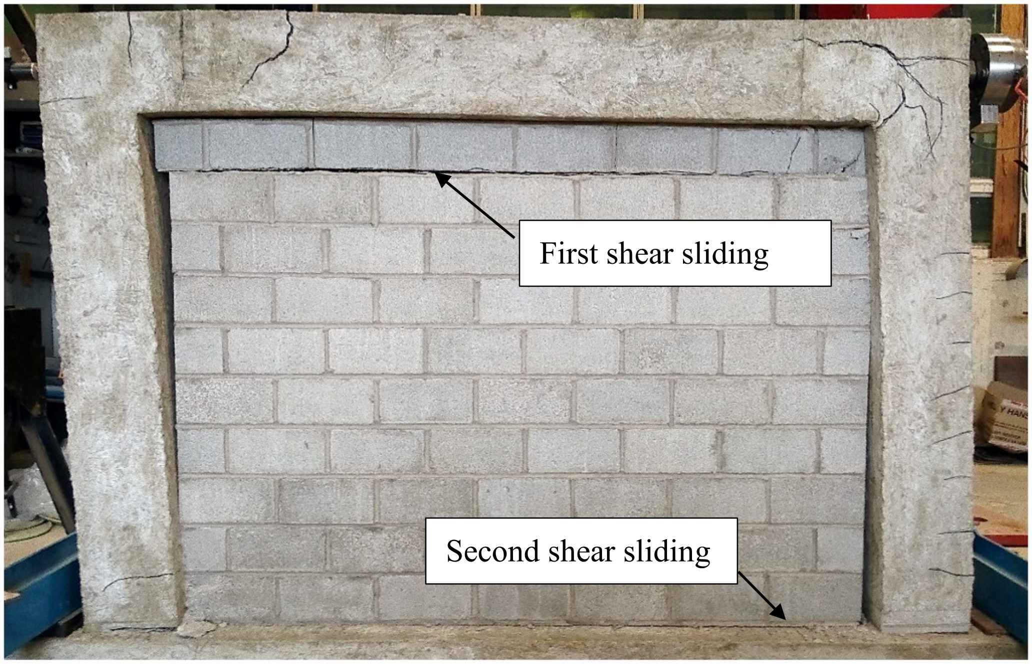

(a) Overview

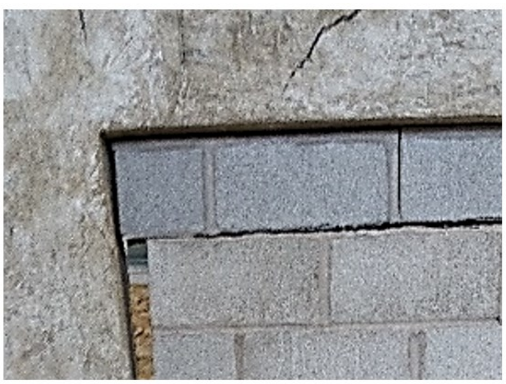

(b) Left upper corner

(c) Right upper corner

(d) Left lower corner

(e) Right lower corner

Figure 4.14 Failure pattern of specimen IFSG7

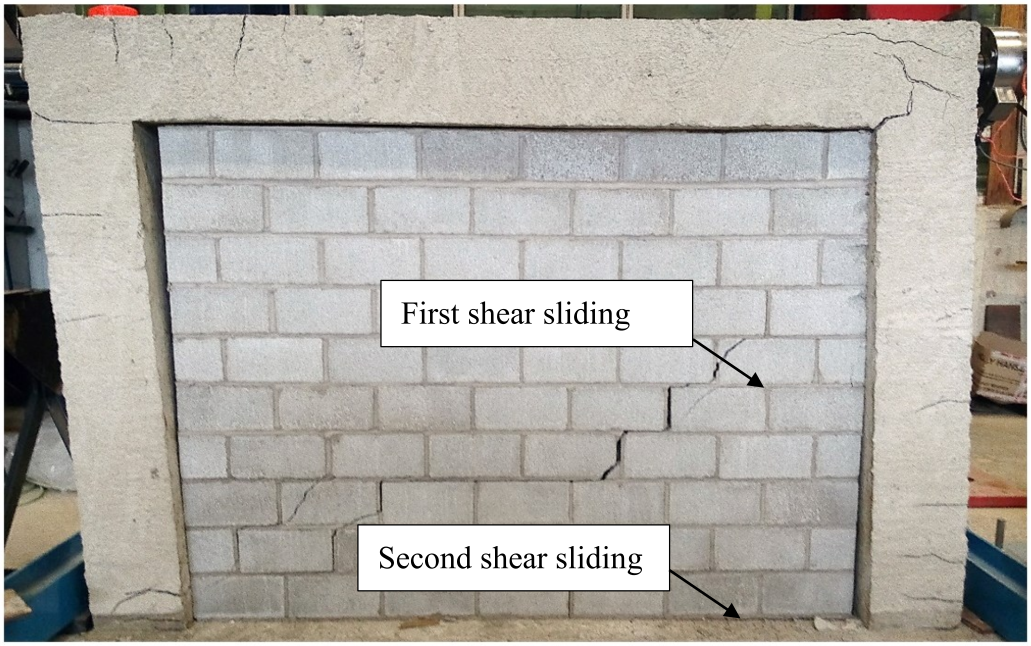

(a) Overview

(b) Left upper corner

(c) Right upper corner

(d) Left lower corner

(e) Right lower corner

Figure 4.15 Failure pattern of specimen IFSG12

4.5 EVALUATION OF INTERFACIAL GAP EFFECTS

Table 4.8 presents the test results of all the frame specimens. The table shows that, compared with the bare frame (BF), the presence of infills significantly increased the stiffness and ultimate strength of the infilled frames regardless of whether gaps were present. In the case of the infill frame with no gaps (IFNG), the strength increase, when compared with the bare frame, was about 132% whereas the increases in the initial stiffness and ultimate stiffness were about 98% and 618%, respectively. Even when gaps were present with the studied magnitudes and locations, these increases due to the infill were pronounced.

Table 4.8 Test results of frame specimens

ID	f'_m (MPa)	f'_c (MPa)	K_{ini} (kN/mm)	K_{cra} (kN/mm)	K_{ult} (kN/mm)	P_{cra} (kN)	P_{ult} (kN)	Initiation of failure	Final failure mode
BF	-	42.3	20.2	-	1.7	-	57.7	-	-
IFNG	16.7	42.3	39.9	18.2	12.2	101.9	133.6	DC	CC
IFTG7	16.7	42.3	28.7	10.0	7.3	100.0	129.6	DC	CC
IFTG12	16.7	42.3	28.6	16.4	3.4	44.3	103.6	DC	CC
IFSG7	17.1	45.3	27.3	9.4	6.5	90.3	135.2	SS	CC
IFSG12	17.1	45.3	27.1	7.1	2.5	64.9	114.2	SS	CC

Note: DC stands for diagonal cracking; SS stands for shear sliding; CC stands for corner crushing.

4.5.1 Effects of Top Interfacial Gaps

Figure 4.16 plots the load vs. lateral displacement curves for evaluating the top gap effects. It showed that the initial stiffnesses of specimen IFTG7 and IFTG12 were almost identical, being 28.7 kN/mm and 28.6 kN/mm respectively, which were lower than that of specimen IFNG with a value of 39.9 kN/mm. This represented a 28% reduction. This indicated that the presence of a top gap did result in reduction in the initial stiffness but the two gap magnitudes studied did not cause noticeable variation in the initial stiffness. This was in line with the finding from the finite element analysis conducted by Nazief (2014), in which no significant changes of the initial stiffness of masonry infilled RC frames were observed when the top gap size varied from 5, 7, 10 to 15 mm. For the ultimate stiffness, the corresponding reduction was 40% for specimen IFTG7, and 72% for specimen IFTG12, when compared with specimen IFNG. This was expected since the specimen with a greater gap developed more extensive diagonal cracking at the failure. The crack stiffnesses of specimen IFTG7 and IFTG12 were still lower than specimen IFNG, while specimen IFTG7 showed the lowest among these three. This was attributed to the fact that specimen IFTG12 developed the first infill diagonal cracking much earlier in the loading history than the other two specimens when the infilled systems were still in the elastic range. For the strength comparison, both Table 4.8 and Figure 4.17 showed that a 7 mm top gap had little influence on either the first crack load or the ultimate load, where the reductions were only

2% and 3%, respectively. However, a 5 mm increase in the top gap to 12 mm resulted in 57% and 22% reductions in the first crack load and the ultimate load, respectively. The trend found in this study that the ultimate load decreased more as the top gap size increased was in line with the trend of the ultimate load of masonry infilled RC frames found in the study of Nazief (2014). But the exact values of the ultimate load reductions were different. This could be due to that the relative stiffnesses of the frame and the infill as well as the properties of the materials were different in these two studies. Also for the 12 mm top gap case, in the finite element analysis conducted by Ng'andu (2006), 20% reduction on the initial stiffness but little reduction on the ultimate load of the masonry infilled steel frame caused by a 12 mm top gap were observed. It should be noted that the bounding frame was steel and the masonry infill wall was made of calcium silicate element in the study of Ng'andu (2006), which could explain why the results were different from this study.

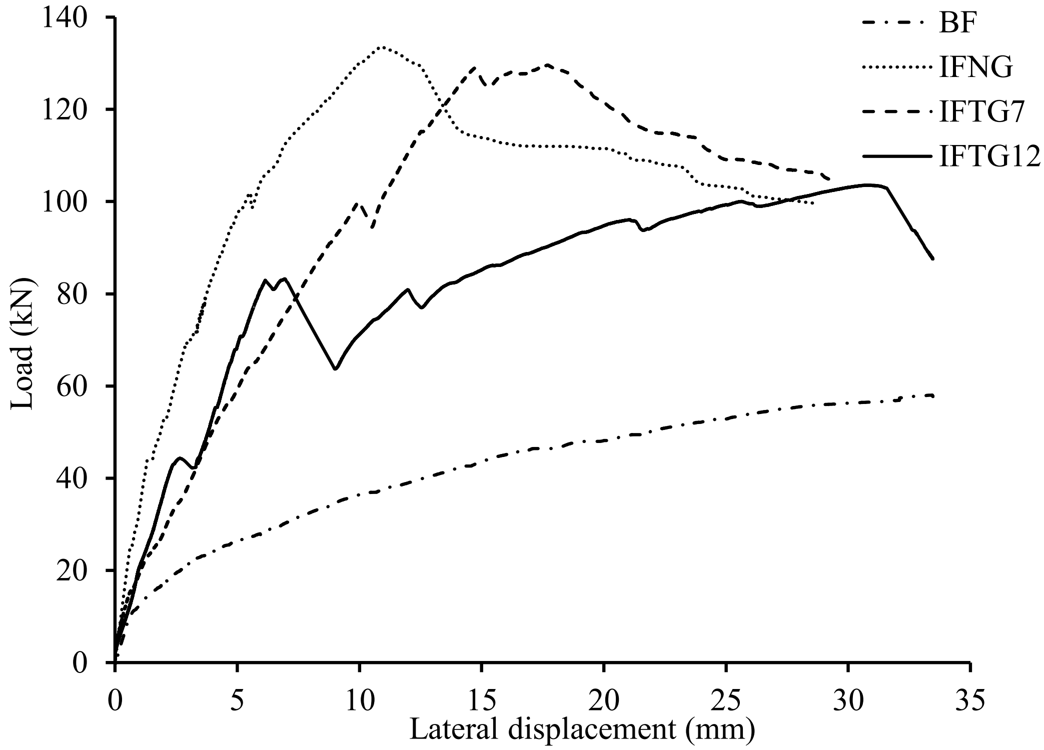

Figure 4.16 Load vs. displacement curves for evaluating top interfacial gap effects

4.5.2 Effects of Side Interfacial Gaps

When comparing the specimens with side gaps versus those with a top gap or without gaps, one distinctive characteristic was that the shear sliding, rather than diagonal cracking, initiated the final failure of these specimens. Figure 4.17 plots the load vs. lateral displacement curves for evaluating the side gap effects. It was found that the initial stiffnesses of specimen IFSG7 and IFSG12 were almost identical, with a value of 27.3 kN/mm and 27.1 kN/mm, respectively. They were lower than that of specimen IFNG

(32% lower) due to the presence of side gaps, but higher than that of the bare frame due to the friction at the interface of the infill and the frame top beam. After the initial stage and before the frame column achieved contact with the infill at the loaded side, the system behaved like the bare frame. After the contact was made, the stiffness showed an abrupt increase due to the contribution of the infill. Further load increase resulted in shear sliding as discussed earlier, which was reflected as the first pronounced load drop on the load vs. displacement curve. A comparison of the crack stiffness showed that the greater the gap, the more crack stiffness reduction. Compared with specimen IFNG, the crack stiffness reductions were 45% and 61% for specimens IFSG7 and IFSG12, respectively. Similar reduction trend was also observed for the ultimate stiffness with respective reduction magnitudes of 47% and 80% for specimens IFSG7 and IFSG12, respectively. A different observation was made for the crack stiffness of the specimens with side gaps compared with the specimens with a top gap where a 12 mm top gap resulted in a lower crack stiffness reduction than a 7 mm top gap did. For specimen IFSG7 and IFSG12, the infill had to deflect laterally 3.5 mm and 6 mm respectively at the loaded side to engage the infill in the system stiffness, as shown in Figure 4.17. A frame analysis on the bare frame showed that the elastic lateral deformation of the frame is approximated at 7 mm (calculation was shown in Appendix B). This indicated that the frame columns of specimen IFSG12 were closer to inelastic behaviour than those of specimen IFSG7. This was believed to attribute to the lower crack stiffness of specimen IFSG 12 compared with specimen IFSG7.

For the strength comparison, the 7 mm side gaps with 3.5 mm at each side caused 11% reduction in the first crack load but the ultimate load of the specimen IFSG7 was slightly higher (1%) than that of specimen IFNG. This anomaly was believed to be attributed to the fact that the frame concrete strength of specimen IFSG7 was higher (7%) than that of specimen IFNG, and the infill strength of specimen IFSG7 was also slightly higher (6%) than that of specimen IFNG. The 12 mm side gaps with 6 mm at each side resulted in 36% and 15% reductions in the first crack load and ultimate load, respectively.

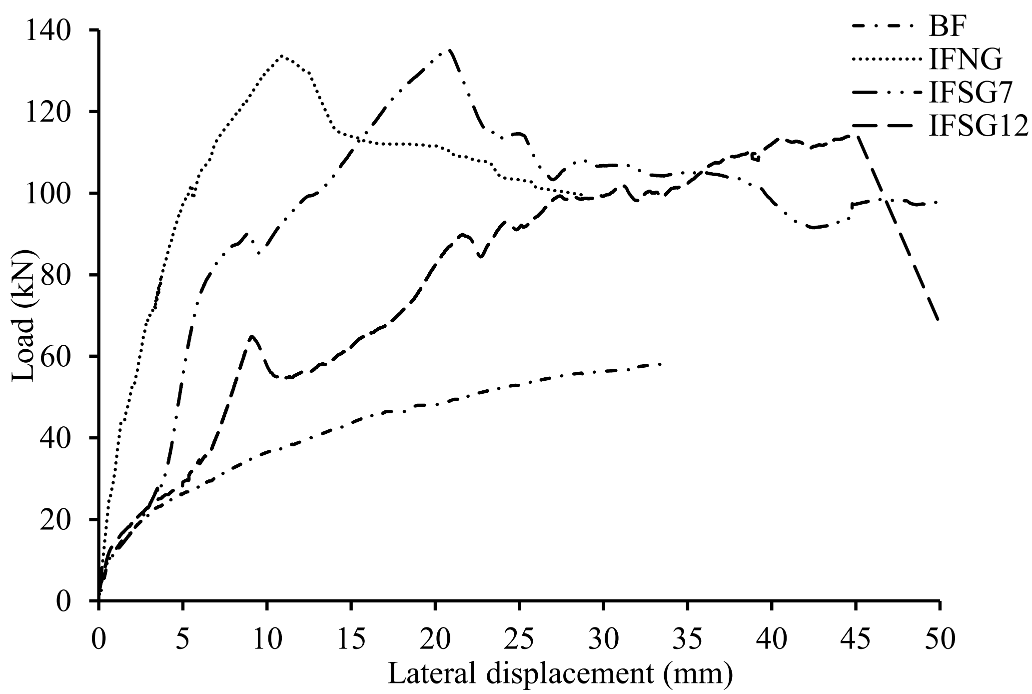

Figure 4.17 Load vs. displacement curves for evaluating side interfacial gap effects

4.5.3 Effects of Gap Locations

To evaluate the effect of the gap location, the results of the infilled frames with the same total size of gaps were compared and analyzed. Figure 4.18 and 4.19 plot the load vs. lateral displacement curves to evaluate the gap location effect of gaps of 7 and 12 mm, respectively. As shown in these two figures below and Table 4.8, the side gap caused more decreases in the initial, crack, and ultimate stiffness than the top gap of the same size did, thus making the system more flexible with a larger displacement at the ultimate load. However, when comparing the strength, it seemed that the gaps of 7 mm, regardless of the gap location, did not result in any significant reduction in ultimate load. The gaps of 12 mm resulted in more pronounced reduction in the ultimate load. This reduction was more significant for the top gap than for the side gap although the ultimate load for specimen IFSG12 was achieved at a much greater deflection compared with specimen IFTG12.

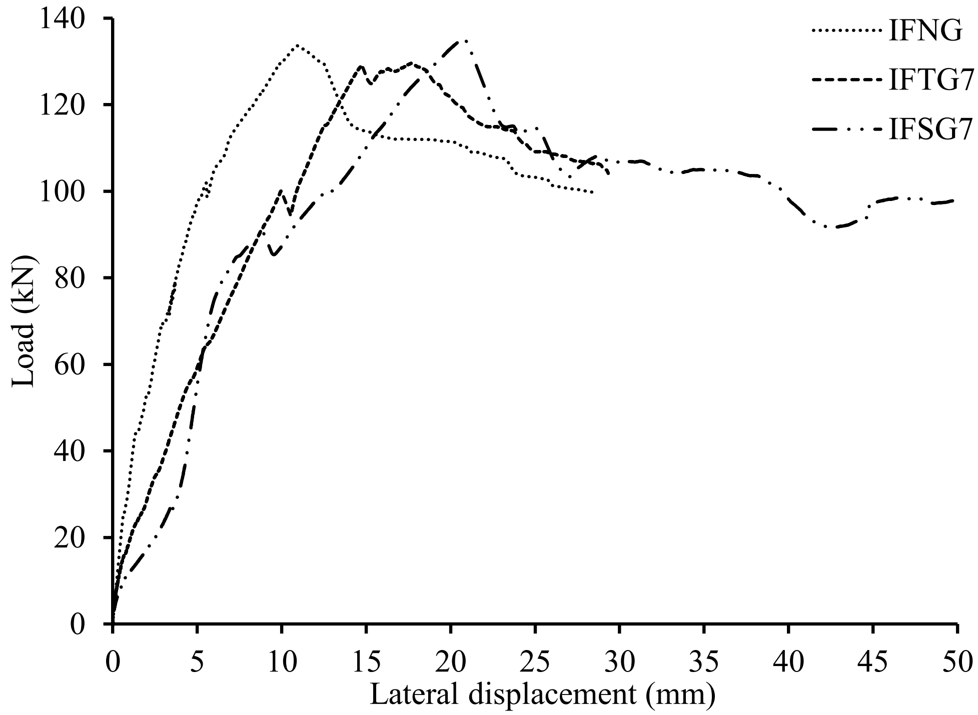

Figure 4.18 Load vs. displacement curves for evaluating location effects of 7 mm gaps

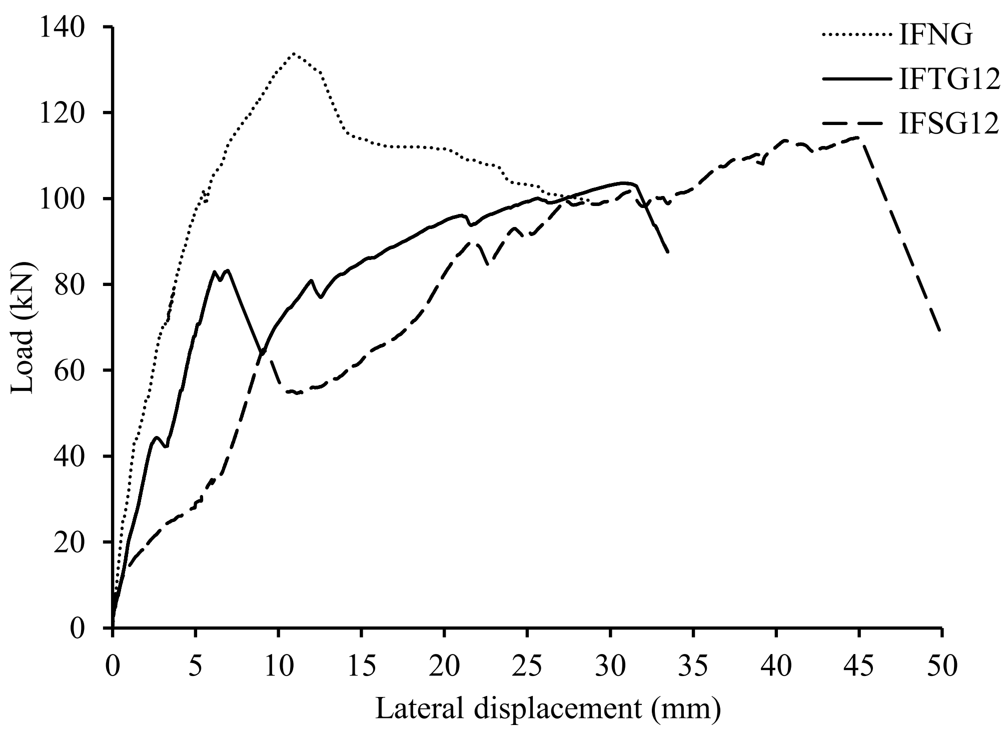

Figure 4.19 Load vs displacement curves for evaluating location effects of 12 mm gaps

4.5.4 Summary on Gap Effects

With the available test results, relationships between the gap size and the normalized initial stiffness and strength can be plotted in Figure 4.20 and 4.21, respectively. The vertical axis of Figure 4.20 represented the stiffness values normalized using the initial stiffness of specimen IFNG. If a simple linear relationship was assumed, the average stiffnesses of the infilled frames with gaps of 7 or 12 mm were roughly the same and the stiffness reductions compared with the infilled frame with no gaps were about 30% for these two gap magnitudes. Hence the reduction factor for gaps of 9.5 mm would be around 0.7. Similarly, the vertical axis of Figure 4.21 represented the strength values normalized using the ultimate load shared by the infill only of specimen IFNG. As opposed to the code provisions, the infilled specimens still had appreciable strength when the gap size was 12 mm. For an assumed linear correlation, the figure showed a reduction factor of around 0.7 for gaps of 9.5 mm and a reduction factor of 0.5 for gaps of 12 mm.

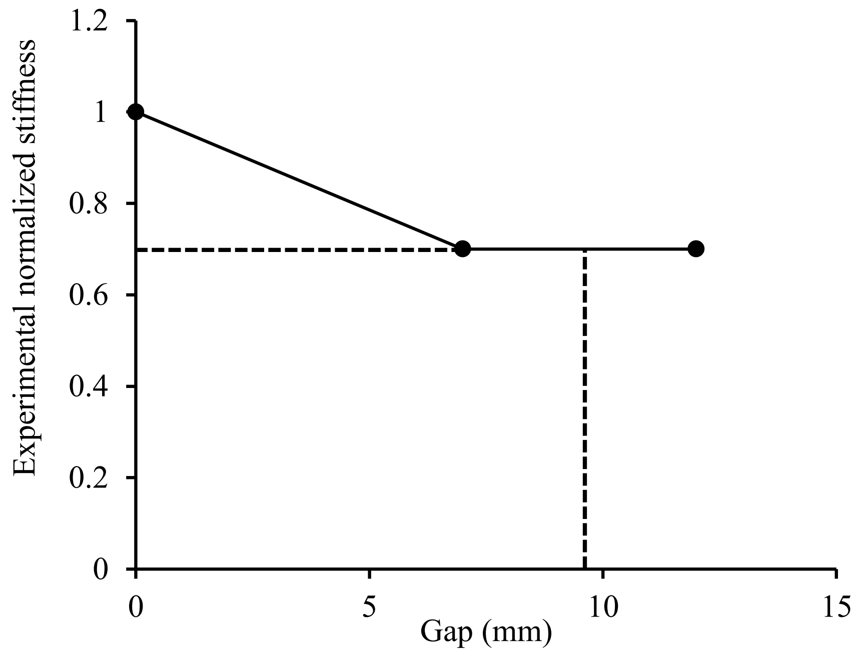

Figure 4.20 Relationship between the gap size and the normalized stiffness

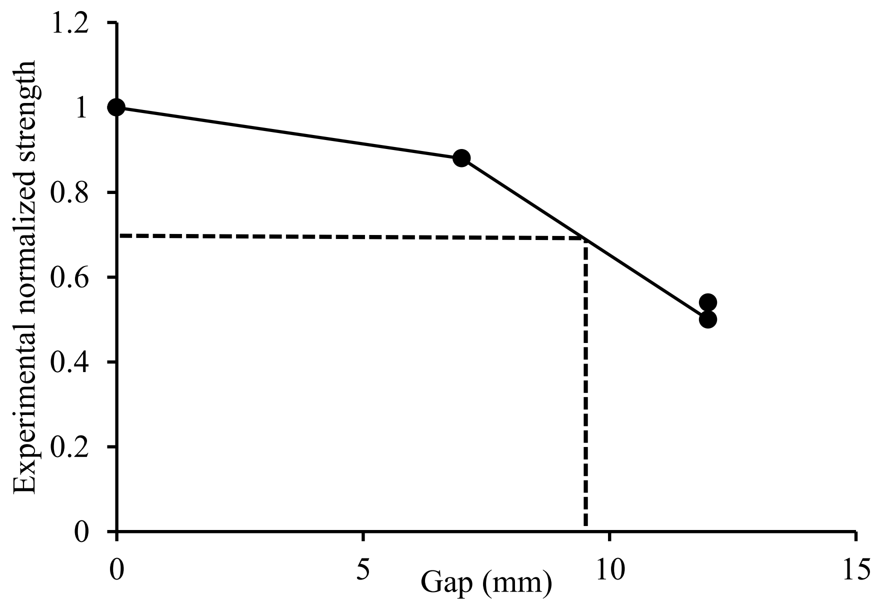

Figure 4.21 Relationship between the gap size and the normalized strength

4.5.5 Storey Drift and Ductility

To have an overall understanding of the gap effect, in addition to the crack strength and ultimate strength, the loads of the frame specimens at a specified drift level were also compared. The allowable storey drifts are 1%, 2%, and 2.5% of the storey height for post-disaster buildings, schools, and all other buildings according to National Building Code of Canada (2010) (NBCC 2010). Table 4.9 summarizes the loads of all the frame specimens obtained at these three drift levels, termed as P_{d1}, P_{d2} and P_{d3}, respectively.

Table 4.9 Test results of frame specimens

ID	f'_m (MPa)	f'_c (MPa)	P_{d1} (kN)	P_{d2} (kN)	P_{d3} (kN)	Δ_y (mm)	Δ_u (mm)	R
BF	-	42.3	39.0	52.1	56.3	16.9	33.5	2.0
IFNG	16.7	42.3	130.1	104.1	100.0	6.8	11.0	1.6
IFTG7	16.7	42.3	110.6	112.8	139.8	10.5	17.7	1.7
IFTG12	16.7	42.3	80.8	97.9	103.0	16.8	30.8	1.8
IFSG7	17.1	45.3	97.7	113.9	106.8	14.7	20.7	1.4
IFSG12	17.1	45.3	56.0	91.9	99.3	23.8	45.0	1.9

These three storey drifts resulted in lateral deflections of 12.0, 23.9, and 29.9 mm respectively for the height of the frame (1195 mm) considered in this study. The loads with respect to the storey drifts were obtained from the load vs. displacement curve of each specimen as shown in Figure 4.22 again for clarity. As shown in Table 4.9, only at the 1% drift level corresponding to post-disaster buildings, the presence of gaps of 7 or 12 mm was found to cause marked reduction in the load, in the order of 20.0% and 47.5%, respectively. For the 2% and 2.5% drift levels corresponding to schools and all other buildings, reductions were not as significant and in some cases even higher loads were observed for the gapped specimens. Combining the discussion with respect to the gap effect on the ultimate load, the above discussion shows that the gap effect on the capacity of the infilled frames is dependent on the limit states in question. If the requirement for the drift displacements is stringent, the use of gapped infilled frames needs to be carefully examined despite the fact that they may have sufficient ultimate capacity.

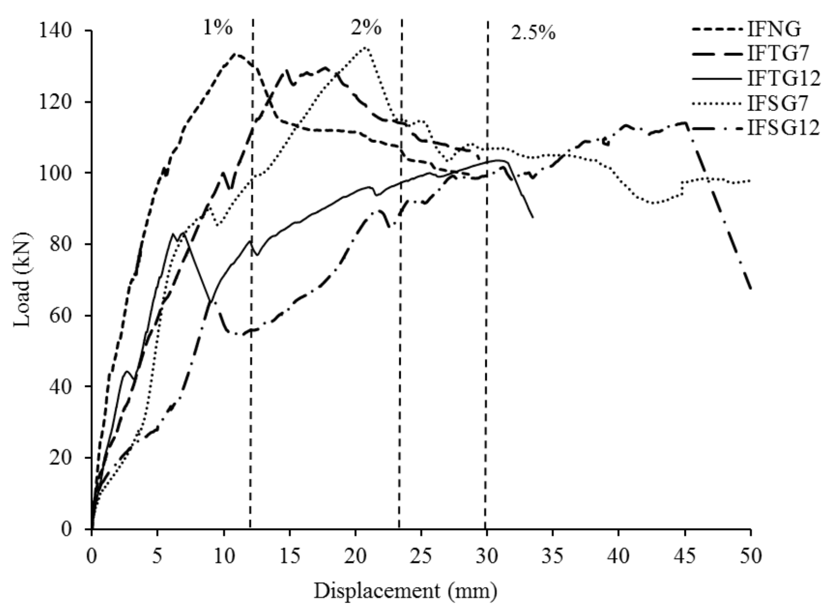

Figure 4.22 Load vs. displacement curves of infilled frame specimens

Also included in Table 4.9 is the displacement ductility factor calculated for each specimen. Ductility is a measure of the capacity of a structure or a member to undergo deformation beyond the yield level, while maintaining most of its load-carrying capacity. When seismic loads are considered, structures or members are always designed to have a certain amount of ductility so that they are able to absorb and dissipate earthquake energy by plastic deformations. Once the ductility demands are met, the structure can be designed at a reduced seismic load. The current building code NBCC 2010 permits that the design seismic loads be reduced by a factor of 1 to 5 depending on the type of seismic resisting systems used. The typical ductility factors used in the design for moderately ductile moment-resisting RC frames and unreinforced masonry are 2.5 and 1.0, respectively. However, masonry infilled frames are not explicitly listed as a type of seismic load resisting systems. It should be pointed out that the ductility factor is more appropriately discussed in the context of seismic loading application of specimens. Although the load vs. displacement curves are obtained under the static loading, it is still worthwhile to compare the ductility of masonry infills if such curves are assumed to be similar to the envelope curve of the hysteresis load vs. displacement responses under cyclic loading.

In this case, the ductility factor is calculated as the ratio of the displacement at the ultimate load to the displacement at 80% of the ultimate load in the ascending part of the curve, termed as Δ_u and Δ_y respectively, as illustrated in Figure 4.23. This approach has been adopted in the evaluation of ductility by several researchers (Salonikios et al., 2000; Carrillo et al., 2014; Tawfik et al., 2014). Thus the ductility factor is computed using Equation 4.1 and the results are listed in Table 4.8.

$$R = \Delta_u / \Delta_y \qquad [4.1]$$

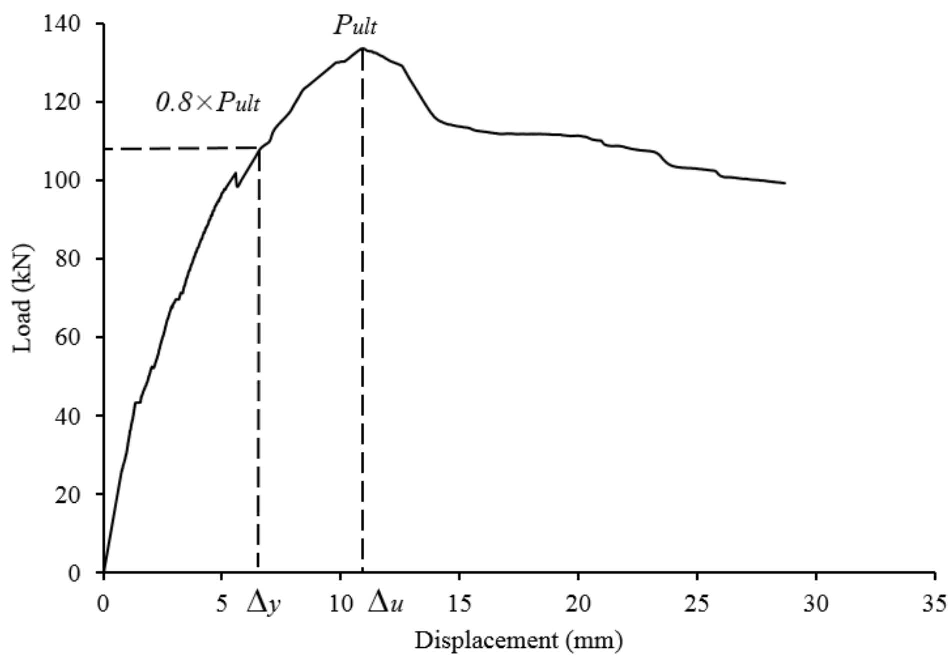

Figure 4.23 Illustration of Δ_y and Δ_u

As shown in Table 4.9, the ductility factor of the bare frame was calculated to be about 2.0; and the average of the ductility factors for the infilled specimens was determined to be about 1.7. The latter value is greater than 1.0 which is assigned for unreinforced masonry in NBCC 2010, indicating that the unreinforced masonry bounded by RC frames has much improved ductility. Secondly, the ratio of the ductility factors of the bare frame and the infilled frames obtained from this study is around 2/1.7=1.2, which is much lower than 2.5 as suggested by NBCC 2010. This indicates that the ductility of masonry infilled frames can be comparable to that of the RC bare frame. It is recognized that while more testing is needed, the study so far suggests that masonry infilled frames can be effectively used as seismic resisting systems in a structure.

CHAPTER 5 EVALUATION OF DESIGN AND ANALYTICAL METHODS

5.1 INTRODUCTION

In this chapter, the experimentally obtained stiffness and strength of the infilled frame specimens are used to assess the performance of several analytical methods presented in Chapter 2 as well as the design methods specified in CSA S304.1 and MSJC 2011. Although all the methods are intended for the infills without gaps, the comparison is hoped to provide information on the reduction factor of the stiffness and strength for the infills with gaps.

5.2 STIFFNESS EVALUATION

Both these two aforementioned design codes as well as several analytical methods provide equations to calculate the width of the diagonal strut (presented in Chapter 2). Once the width is determined, a commercial software SAP2000 is used to perform a frame analysis of the infilled frame with the obtained strut width. In the analysis of the infilled frame, a unit load (1kN) was placed at the top frame beam level and the corresponding lateral displacement (Δ mm) at the load point was obtained. Then the stiffness of the infilled frame was determined as the inverse of the lateral displacement.

Table 5.1 lists the material and geometrical properties of the specimens used in the evaluation. It is noted both CSA S304.1 and ASTM C1314 specify a height-to-thickness correction factor for experimentally determined f'_m. For the prisms tested in this study, the correction factors were approximately 1.0 for both the Canadian and American standards. Hence the experimentally determined compressive strength of the prism was directly used as the specified compressive strength of the infill. The modulus of elasticity of the infill was taken as 850 f'_m according to CSA 304.1. The modulus of elasticity of the concrete was used as the frame modulus, E_f, in the diagonal strut width calculation. The thickness, t_e, is the total face shell thickness of the masonry infill.

Table 5.1 Material and geometrical properties of specimens

ID	h (mm)	l (mm)	f'_m (MPa)	E_m (MPa)	E_f (MPa)	I_b=I_c (x10^6mm)	t_e (mm)
IFNG	980	1350	16.7	14195	28424	87.5	34
IFTG7	980	1350	16.7	14195	28424	87.5	34
IFTG12	980	1350	16.7	14195	28424	87.5	34
IFSG7	980	1350	17.1	14535	29295	87.5	34
IFSG12	980	1350	17.1	14535	29295	87.5	34

5.2.1 CSA S304.1

Table 5.2 summarizes the comparison of the test initial stiffness and the stiffness based on CSA S304.1. For easy reference, the key provisions for the determination of the diagonal strut width specified in CSA S304.1 are summarized in the following.

$$w = \frac{1}{2}\sqrt{{\alpha_h}^2 + {\alpha_L}^2} \le \frac{d}{4} \qquad [5.1]$$

where:

$$\alpha_h = \frac{\pi}{2}\sqrt[4]{\frac{4E_f I_c h}{E_m t_e \sin 2\theta}} \qquad [5.2]$$

$$\alpha_L = \pi\sqrt[4]{\frac{4E_f I_b l}{E_m t_e \sin 2\theta}} \qquad [5.3]$$

It should be reiterated that CSA S304.1 does not contain provisions for the infills with interfacial gaps. The CSA 304.1 values in the table were determined treating the infill as a "normal" infill. For the verification purpose, both the calculated strut width based on the right part of Equation [5.1], w_u, and the design strut width limited to one quarter of the infill diagonal length, w_m, were used in the CSA stiffness calculation for all the infilled frame specimens.

Table 5.2 Comparison of test initial stiffness and CSA stiffness

ID	Test	CSA S304.1					
	K_{ini} (kN/mm)	w_u (mm)	K_{CSA-u} (kN/mm)	K_{CSA-u} / K_{ini}	w_m (mm)	K_{CSA-m} (kN/mm)	K_{CSA-m} / K_{ini}
IFNG	39.9	715	122.0	3.06	417	82.0	2.06
IFTG7	28.7	715	122.0	4.25	417	82.0	2.86
IFTG12	28.6	715	122.0	4.27	417	82.0	2.87
IFSG7	27.3	716	125.0	4.58	417	84.0	3.08
IFSG12	27.1	716	125.0	4.61	417	84.0	3.10
			Avg.	4.15			2.79
			COV	15%			15%

Note: K_{CSA-u} was calculated by using w_u; K_{CSA-m} was calculated by using w_m.

As shown in Table 5.2, CSA S304.1 overestimated the initial stiffness of the specimen with no gaps (IFNG) by about 3.06 times with the use of the calculated strut width and by about 2.06 times with the design strut width. And this overestimation became more pronounced for the specimens with gaps. Regardless of which diagonal strut width to use, the code values grossly overestimated the stiffness of the infilled system. This was attributed to an overestimation of the diagonal strut width. Relatively low COV values (15%) for the design-to-test ratios indicated that the overestimation was consistent for all the specimens. Further frame analysis was then conducted to determine the strut width that can compare better with the test results. It was found that reducing the calculated strut width by 60% gave a design-to-test stiffness ratio of about 1.5 for the specimen without gaps. To maintain the similar design-to-test stiffness ratio of about 1.5, the stiffness of the specimens with gaps needs to be reduced by 30% on average from the specimen without gaps, which is in line with the discussion presented in Chapter 4. This 30% reduction on the system stiffness corresponds to a 50% reduction on the strut width for the gapped specimens. The results are shown in Table 5.3, where w_n stands for the strut width modified by the new reduction factors; K_{CSA-n} stands for the stiffness using the new modified strut width based on the CSA method.

Table 5.3 Comparison of test initial stiffness and modified stiffness

ID	Test	CSA S304.1		
	K_{ini} (kN/mm)	w_n (mm)	K_{CSA-n} (kN/mm)	K_{CSA-n} / K_{ini}
IFNG	39.9	286	60.2	1.51
IFTG7	28.7	143	42.7	1.49
IFTG12	28.6	143	42.7	1.49
IFSG7	27.3	143	43.9	1.61
IFSG12	27.1	143	43.9	1.62

5.2.2 MSJC 2011

Table 5.4 summarizes the comparison of the test initial stiffness and the stiffness based on MSJC 2011. For easy reference, the key provision for the determination of the diagonal strut width in MSJC 2011 is summarized in the following.

$$w = \frac{0.3}{\lambda \cos\theta} \qquad [5.4]$$

where,

$$\lambda = \sqrt[4]{\frac{E_m t_e \sin 2\theta}{4 E_f I_c h}} \qquad [5.5]$$

MSJC 2011 states that the infill stiffness shall be reduced by 50% for infilled frames with a top gap less than 9.5 mm. Here for the verification purpose, the 50% reduction factor was implemented to the infill stiffness based on Equation [5.4] of specimen IFTG7, IFTG12, IFSG7, and IFSG12 in the MSJC stiffness calculation.

Table 5.4 Comparison of test initial stiffness and MSJC stiffness

ID	Test	MSJC 2011		
	K_{ini} (kN/mm)	w (mm)	K_{MSJC} (kN/mm)	K_{MSJC} / K_{ini}
IFNG	39.9	142	42.7	1.07
IFTG7	28.7	71	32.2	1.12
IFTG12	28.6	71	32.2	1.13
IFSG7	27.3	71	33.0	1.21
IFSG12	27.1	71	33.0	1.22

As shown in Table 5.4, the MSJC stiffness of the specimen with no gaps (IFNG) agreed quite well with the experimental initial stiffness with a design-to-test ratio of about 1.07. After implementing the 50% reduction factor for w, the design-to-test stiffness ratios for the specimens with gaps were averaged about 1.17. It seems that the 50% reduction is reasonable. It should be pointed out that the MSJC 2011 considers the infills with a top gap of greater than 9.5 mm as non-participating infills. The results showed, however, there was no significant variation in the stiffness when the top gap varied from 7 to 12 mmm.

5.2.3 Other Methods

The performance of several analytical methods presented in Chapter 2 for the calculation of the diagonal strut width is evaluated here. For easy reference, those analytical methods used are summarized in Table 5.5.

Table 5.5 Analytical methods used for stiffness comparisons

References	Equations for strut width
Stafford-Smith and Coull (1991)	$w = \frac{d}{10}$
Angel (1994)	$w = \frac{d}{8}$
Mainstone (1971)	$w/d = 0.115(\lambda h')^{-0.4}$ $4 \le \lambda h' \le 5$ $w/d = 0.11(\lambda h')^{-0.3}$ $\lambda h' \ge 5$
Liauw and Kwan (1984)	$w = \min\left(\frac{0.86h\cos\theta}{\sqrt{\lambda h}}, 0.45h\cos\theta\right)$
Al-Chaar (2002)	$w\text{=}0.0835Bd\left(1+\frac{2.574}{\lambda h'}\right)$ for $\frac{l}{h} \ge 1.5$ $w\text{=}0.1106d\left(1+\frac{6.027}{\lambda h'}\right)$ for $\frac{l}{h}\text{=}1.0$

Table 5.6 lists the strut widths calculated based on these analytical methods. Table 5.7 lists the comparison of experimental stiffness and the stiffness based on these analytical methods.

Table 5.6 Strut widths based on analytical methods

ID	*w* (mm)				
	Mainstone (1971)	Liauw & Kwan (1984)	Stafford-Smith & Coull (1991)	Angel (1994)	Al-Chaar (2002)
IFNG	127	357	167	209	383
IFTG7	127	357	167	209	383
IFTG12	127	357	167	209	383
IFSG7	127	348	167	209	383
IFSG12	127	348	167	209	383

Table 5.7 Comparison of test stiffness and stiffness based on analytical methods

ID	K_{ini} (kN/mm)	K/K_{ini}				
	Test	Mainstone (1971)	Liauw & Kwan (1984)	Stafford-Smith & Coull (1991)	Angel (1994)	Al-Chaar (2002)
IFNG	39.9	1.02	1.84	1.16	1.31	1.93
IFTG7	28.7	1.41	2.56	1.61	1.83	2.68
IFTG12	28.6	1.42	2.57	1.62	1.83	2.69
IFSG7	27.3	1.52	2.71	1.74	1.97	2.91
IFSG12	27.1	1.53	2.73	1.76	1.98	2.93
Avg.	-	1.38	2.48	1.58	1.78	2.63
COV	-	15%	15%	15%	15%	15%

As shown in Table 5.7, all the methods overestimated the stiffness of the infilled specimens to various degrees. The method proposed by Mainstone (1971) gave the lowest value of the strut width which in turn led to the best stiffness estimate with an average test-to-analytical ratio of about 1.38. As shown in Table 5.6, the strut width value based on Mainstone (1971) was similar to that based on MSJC 2011.

5.3 STRENGTH EVALUATION

5.3.1 CSA S304.1

For specimen IFNG, IFTG7, and IFTG12, the corner crushing failure was initiated by diagonal cracking; while for specimen IFSG7 and IFSG12, the failure was initiated by shear sliding along the bed joints. CSA 304.1 provides a set of equations to calculate the infill strength according to three failure modes, namely, diagonal cracking, shear sliding, and corner crushing. Thus when evaluating CSA S304.1, the experimental loads with respect to each failure state were compared with the code strength calculated based on the corresponding design equation.

The following three failure modes are designated in CSA 304.1 and the corresponding equations are provided.

(a) Diagonal cracking failure mode

$$V_r = \phi_m (v_m b_w d_v + 0.25 P_d)\gamma_g \leq 0.4\phi_m \sqrt{f'_m} b_w d_v \gamma_g \qquad [5.6]$$

where,

$$v_m = 0.16(2 - \frac{M_f}{V_f d})\sqrt{f'_m} \qquad [5.7]$$

For squat walls (h/l<1), the upper limit in Equation [5.6] may be increased to:

$$V_r \leq 0.4\phi_m \sqrt{f'_m} b_w d_v \gamma_g (2 - \frac{h}{l}) \qquad [5.8]$$

where V_r is the ultimate load; ϕ_m is the resistance factor for masonry; v_m is the shear strength of the masonry; b_w is the actual thickness of the web of the infill wall; d_v is the actual depth of the infill wall in the direction of shear considered; P_d is the axial compressive load on the section considered; γ_g is the factor to account for partially grouted and un-grouted walls constructed of units that are not solid; M_f is the factored moment at the section considered; V_f is the factored shear at the section considered.

(b) Shear sliding failure mode

For sliding along a bed joint:

$$V_r = 0.16\phi_m \sqrt{f'_m} A_{uc} + \phi_m \mu P_1 \qquad [5.9]$$

where A_{uc} is the un-cracked portion of the effective cross-sectional area providing shear bond capacity; μ is the coefficient of friction on the interface between the frame and infill;

P_l is the minimum compressive force acting normal to the sliding plane.

(c) Corner crushing failure mode

$$V_r = \frac{l}{\sqrt{h^2/l^2}} P_r \qquad [5.10]$$

where,

$$P_r = \phi_m \chi (0.85 f'_m) w (2t_f - r) \qquad [5.11]$$

$$r = (\frac{t}{2} + e) - \frac{1}{2}\sqrt{t^2 + 4te + 4e^2 - 16et_f} \qquad [5.12]$$

$$e = \frac{r(t-r)}{2(2t_f - r)} \qquad [5.13]$$

where P_r is the factored axial load resistance; χ is the factor to account for direction of compressive stress in a masonry member relative to the direction used for the determination of f'_m; t_f is the thickness of the flange of the concrete masonry unit; r is the radius of gyration; e is the eccentricity of the load.

Table 5.8 presents the comparison of the experimental and CSA first crack strengths. The experimental crack load was obtained directly by subtracting the bare frame load from the infilled specimen load at the described failure state. The design crack load at which the first major diagonal crack occurred of specimen IFNG, IFTG7, and IFTG12 was calculated using Equation [5.6]; the sliding load at which the shear sliding along the bed joints occurred of specimen IFSG7 and IFSG 12 was calculated using Equation [5.9]. It should be noted that all the resistance factors in the above equations were assumed to be unity to facilitate the comparison with raw experimental data.

Table 5.8 Comparison of first crack strength from tests and CSA S304.1

ID	Test			CSA S304.1	
	System	Frame	Infill		
	P_{cra} (kN)	P_{frame} (kN)	P_{infill} (kN)	$P_{CSA\text{-}cra}$ (kN)	$P_{CSA\text{-}cra}$ / P_{infill}
IFNG	101.9	27.3	74.6	42.0	0.56
IFTG7	100.0	36.4	63.6	42.0	0.66
IFTG12	44.3	20.2	24.1	42.0	1.74
IFSG7	90.3	35.8	54.5	88.7	1.63
IFSG12	64.9	34.9	60.0	88.7	1.48

Table 5.8 shows that for diagonal cracking, CSA S304.1 underestimated the first crack strength of the specimen without gaps (IFNG) and the specimen with a 7 mm top gap (IFTG7) by an average of about 40%. This was expected since the previous discussion

showed that a 7 mm top gap did not have significant effects. However, the crack strength of the specimen with a 12 mm top gap (IFTG12) was overestimated by more than 70% approximately. If a reduction factor of 0.5 is applied, the design-to-test ratio will be about 0.87, which is more reasonable. In the case of shear sliding strength, CSA S304.1 overestimated the sliding load for the gapped specimens (IFSG7 and IFSG12) by about 56% on average. This suggests that shear sliding induced by side gaps may occur at a much lower load than an infill without gaps. A 0.5 reduction factor will reduce the average design-to-test ratio to about 0.78 for the two side gap magnitudes.

Table 5.9 presents the comparison of the experimental and CSA ultimate strengths. The design ultimate load of all the specimens was calculated using Equation [5.10] as all the specimens failed in corner crushing manner. Again, the two code values were calculated with respect to the two diagonal strut widths, i.e., the calculated width based on the right part of Equation [5.1] (w_u) and the specified limit of d/4 (w_m). $P_{CSA\text{-}u}$ stands for the strength with the use of w_u whereas $P_{CSA\text{-}m}$ stands for the strength with the use of w_m.

Table 5.9 Comparison of ultimate strength from tests and CSA S304.1

ID	Test			CSA S304.1			
	System	Frame	Infill				
	P_{ult} (kN)	P_{frame} (kN)	P_{infill} (kN)	$P_{CSA\text{-}u}$ (kN)	$P_{CSA\text{-}u}$ / P_{infill}	$P_{CSA\text{-}m}$ (kN)	$P_{CSA\text{-}m}$ / P_{infill}
IFNG	133.6	35.6	98.0	113.7	1.16	65.7	0.67
IFTG7	131.1	44.5	86.6	113.7	1.31	65.7	0.76
IFTG12	104.7	56.1	48.6	113.7	2.34	65.7	1.35
IFSG7	135.2	48.2	87.0	116.6	1.34	67.3	0.77
IFSG12	113.1	60.0	53.1	116.6	2.20	67.3	1.27
				Avg.	1.67		0.96
				COV	33%		33%

As shown in Table 5.9, the CSA ultimate strength with the use of the calculated strut width agreed well with the experimental ultimate strength of the specimen with no gaps (IFNG), with a design-to-test ratio of about 1.16; it also agreed reasonably well with the specimens with 7 mm top or side gaps (IFTG7 and IFSG7), with design-to-test ratios of about 1.31 and 1.34, respectively. In the case of 12 mm top or side gaps (IFTG12 and IFSG12), CSA S304.1 overestimated the capacity by more than two times. With the use of the design strut width (w_m), the design-to-test ultimate strength ratios of specimen IFNG, IFTG7, and

IFSG7 fell below unity, with an average of about 0.73. However, for the specimens with 12 mm top or side gaps, the overestimation by the CSA S304.1 still existed, with design-to-test ultimate strength ratios being 1.31 on average. Since the conservative estimate of the capacity is more desirable in design, the use of the design strut width (d/4) is better suited than the calculated strut width (w_u) in the strength consideration. Referring to the discussion for the stiffness, the following observations can be made in terms of CSA S304.1. It seems that for the stiffness consideration, the diagonal strut width should be further narrowed to reduce the overestimation by CSA S304.1; but it, in its current form, is acceptable for the strength consideration. When interfacial gaps are concerned, gaps of 7 mm (top or side) can be considered negligible while gaps of 12 mm require a reduction factor of 0.5 to result in a design-to-test ratio of around 0.66, which is comparable to other specimens.

5.3.2 MSJC 2011

MSJC 2011 states that the infill strength, V_r, is taken as the smallest of corner crushing strength, shear sliding strength, and the strength at a horizontal racking displacement of 25 mm. The experimental strength with respect to each state was compared with the code value calculated based on the corresponding criterion as presented in the following. Equation [5.14a] corresponds to the corner crushing failure while Equation [5.14c] corresponds to the shear sliding failure.

$$V_r = \min \begin{cases} \text{(a)} & (6.0\text{in.}) t_e f'_m \\ \text{(b)} & \text{The calculated horizontal component of the force} \\ & \text{in the equivalent strut at a horizontal racking} \\ & \text{displacement of 25mm } (1.0\text{in.}) \\ \text{(c)} & \dfrac{V_n}{1.5} \end{cases} \qquad [5.14]$$

The nominal shear strength, V_n, shall be the determined as follows:

$$V_n = \min \begin{cases} 3.8 A_{nv} \sqrt{f'_m} \\ 300 A_{nv} \\ or \\ 56 A_{nv} + 0.45 N_u \quad \text{if not fully grouted} \\ 90 A_{nv} + 0.45 N_u \quad \text{if fully grouted} \end{cases} \qquad [5.15]$$

where,

$$A_{nv} = 0.8 l t_e \qquad [5.16]$$

where V_n is the nominal shear strength; N_u is the compressive force acting normal to shear surface.

At the first crack point, the infill of specimen IFSG7 and IFSG 12 showed shear sliding cracking along the bed joints, thus Equation [5.14c] was used to calculate the first crack strength; while specimens IFNG, IFTG7, and IFTG12 were omitted in the first crack strength comparison as there is no equation in MSJC 2011 to calculate the diagonal cracking strength. Table 5.10 presents the comparison of the first crack strength from the tests and MSJC 2011. $P_{MSJC\text{-}u}$ stands for the unmodified strength; $P_{MSJC\text{-}m}$ stands for the strength that was reduced by 50%.

Table 5.10 Comparison of first crack strength from tests and MSJC 2011

ID	Test			MSJC 2011			
	System	Frame	Infill				
	P_{cra} (kN)	P_{frame} (kN)	P_{infill} (kN)	$P_{MSJC\text{-}u}$ (kN)	$P_{MSJC\text{-}u}$ / P_{infill}	$P_{MSJC\text{-}m}$ (kN)	$P_{MSJC\text{-}m}$ / P_{infill}
IFNG	101.9	27.3	74.6	-	-	-	-
IFTG7	100.0	36.4	63.6	-	-	-	-
IFTG12	44.3	20.2	24.1	-	-	-	-
IFSG7	90.3	35.8	54.5	14.1	0.26	7.1	0.13
IFSG12	64.9	34.9	60.0	14.1	0.24	7.1	0.12

As shown in Table 5.10, the shear sliding strength of specimen IFSG7 and IFSG12 calculated based on MSJC 2011 was only about 0.25 times on average of the first crack strength from the tests. By implementing the reduction factor, the design-to-test ratio was even lower, which was reduced to about 0.13 on average. This indicates that MSJC 2011 is too conservative in estimating the shear sliding strength.

Table 5.11 lists the comparison of the experimental and MSJC ultimate strengths. At the ultimate point, the infill of all the specimens failed in corner crushing manner, thus Equation [5.14a] was used to calculate the ultimate strength.

Table 5.11 Comparison of ultimate strength from tests and MSJC 2011

ID	Test			MSJC 2011			
	System	Frame	Infill	P_{MSJC-u} (kN)	P_{MSJC-u} / P_{infill}	P_{MSJC-m} (kN)	P_{MSJC-m} / P_{infill}
	P_{ult} (kN)	P_{frame} (kN)	P_{infill} (kN)				
IFNG	133.6	35.6	98.0	86.5	0.88	86.5	0.88
IFTG7	131.1	44.5	86.6	86.5	1.00	43.3	0.50
IFTG12	104.7	56.1	48.6	86.5	1.78	43.4	0.89
IFSG7	135.2	48.2	87.0	88.6	1.00	44.3	0.51
IFSG12	113.1	60.0	53.1	88.6	1.63	44.3	0.83
				Avg.	1.26		0.72
				COV	33%		28%

As shown in Table 5.11, the unmodified MSJC ultimate strength agreed reasonably well with the experimental ultimate strength, with a design-to-test strength ratio of about 0.88 for the specimen without gaps. For the specimens with gaps, the design-to-test ratio was either equal to or greater than unity, indicating that a reduction factor should be introduced to maintain a more desired conservative design. However, the 50% reduction factor (as shown in last column of the table) seems to be harsh for the specimens with 7 mm top or side gaps but works well for the specimens with 12 mm top or side gaps. This confirms the findings presented in the previous section on CSA S304.1.

Table 5.12 provides the comparison of the infill strength obtained at a horizontal displacement of 25 mm from the tests and MSJC 2011. In the case of MSJC 2011, the infill load was calculated through a braced frame analysis using the diagonal strut width (determined by Equation [5.4]). Two scenarios for the cross-sectional properties of the frame members were considered including 1) the original cross-sectional properties and 2) the reduced cross-sectional properties considering the cracking and yielding of the frame. The reduced cross-sectional properties was calculated using the secant stiffness determined from the load vs. lateral displacement curve of the bare frame at a lateral displacement of 25 mm. The secant stiffness was determined to be approximately 10% of the initial stiffness. Note that the 50% reduction factor was applied in both scenarios for the strength of the infills with gaps.

Table 5.12 Comparison of strength at 25 mm deflection from tests and MSJC 2011

ID	Test			MSJC 2011			
	System	Frame	Infill				
	P_{system} (kN)	P_{frame} (kN)	P_{infill} (kN)	$P_{MSJC,1}$ (kN)	$P_{MSJC,1}$ / P_{infill}	$P_{MSJC,2}$ (kN)	$P_{MSJC,2}$ / P_{infill}
IFNG	102.9	51.7	51.2	566.5	11.1	555.4	10.85
IFTG7	109.3	51.7	57.6	283.3	4.92	277.6	4.82
IFTG12	99.9	51.7	48.2	283.3	5.88	277.6	5.76
IFSG7	113.4	51.7	61.7	282.5	4.58	277.5	4.50
IFSG12	91.7	51.7	40.0	282.5	7.06	277.5	6.94

As shown in Table 5.12, the infill load did not vary significantly when either the initial or secant stiffness was used for the frame members. In any case, the 25 mm criterion grossly overestimated the infill capacity for the geometry and materials used. Comparing the strengths corresponding to corner crushing and 25 mm lateral displacement, it seems that the 25 mm lateral displacement criterion may only govern in the situation of both a weak infill bounded by a weak frame.

5.3.3 Other Methods

Several analytical methods (presented in Chapter 2) proposed by previous researchers for calculating the corner crushing load were evaluated here. For easy reference, those analytical methods used were summarized in Table 5.13.

Table 5.13 Analytical method used for strength comparisons

References	Equations for infill strength
Mainstone (1971)	$H_{CC} = 0.56(\lambda h')^{-0.875} f'_m h' t \cot\theta$
Rosenblueth (1980)	$H_{CC} = \frac{2}{3}\alpha_c t f'_m \sec\theta$
Stafford Smith and Coull (1991)	$H_{CC} = f'_m t \frac{\pi}{2}\sqrt[4]{\frac{4E_f I h'}{E_m t}}$
Galanti et al. (1998)	$H_{CC} = f'_m wt\sqrt{1+\alpha_r^{\ 2}}$
Flanagan and Bennett (1999)	$H_{CC} = K_{CC} t f'_m$

Table 5.14 lists the comparison of the ultimate strength from the tests and the analytical methods presented above. It should be pointed out that those studies did not elaborate whether to use the total thickness or the effective thickness of the infill. A preliminary calculation shows that using effective thickness to account for ungrouted hollow blocks used in this research will give more reasonable results. So in this comparison, effective thickness of the infill was used. Also, Galanti et al. (1998) did not provide an equation to calculate the strut width. The strut width used to calculate the values in the table was based

on MSJC 2011 for the Galanti method. For the gapped specimens, a 0.5 reduction factor has been applied to all the values.

Table 5.14 Comparison of ultimate strength from the tests and analytical methods

ID	P_{infill} (kN)	P/P_{infill}				
	Test	Mainstone (1971)	Rosenblueth (1980)	Stafford-Smith (1991)	Galanti (1998)	Flanagan (1999)
IFNG	98.0	1.94	2.86	3.51	1.02	1.43
IFTG7	86.6	1.10	1.62	1.99	0.58	0.81
IFTG12	48.6	1.96	2.89	3.54	1.03	1.44
IFSG7	87.0	1.11	1.65	2.03	0.59	0.82
IFSG12	53.1	1.83	2.71	3.32	0.96	1.35
Avg.	-	1.59	2.34	2.87	0.83	1.17
COV	-	28%	28%	28%	28%	28%

As shown in Table 5.14, the method proposed by Galanti et al. (1998) provided the best estimates of the infill ultimate strength (corner crushing strength in this case) for the specimen without gaps, with a design-to-test strength ratio of about 1.02. The remaining methods all overestimated the ultimate strength to various degrees. For the gapped specimens, if a 0.5 reduction factor was applied, the resulted average of the design-to-test ratios for Galanti et al. (1998) was about 0.83 with a COV of 28%. The other methods still showed an average design-to-test ratio of greater than 1.0, thus making these methods unconservative in design.

CHAPTER 6 SUMMARY AND CONCLUSIONS

6.1 SUMMARY

This research was conducted to investigate the effect of interfacial gaps on the in-plane behaviour of masonry infilled RC frames. Six scaled specimens, including one bare frame, one infilled frame without any gaps, and four infilled frames with different gap situations were tested under a monotonically increased lateral load to failure. All the masonry infills measured 1350 mm long by 980 mm high, resulting in a height-to-length aspect ratio of about 0.73. The average compressive strength of the infill was about 17 MPa. The RC frames consisted of 180×180 mm reinforced square sections for both the columns and the top beam, and 250×250 mm for the bottom beam. The average compressive strength of the concrete was about 44 MPa. The gap situations contained a top gap of 7 mm, a top gap of 12 mm, 7 mm side gaps with 3.5 mm at each side, and 12 mm side gaps with 6 mm at each side. The infill walls were constructed using half scaled standard 200 mm concrete masonry units, and were unreinforced and ungrouted. During the testing, the general behaviour, cracking and failure pattern, and load vs. lateral displacement response were recorded. The effect of both the gap magnitude and location was presented through the discussion of the behaviour, failure mode, stiffness, strength, and ductility of each specimen. The validity of

CSA 304.1 and MSJC 2011 as well as several existing analytical methods for design of infills was assessed using the experimental results.

6.2 CONCLUSIONS

The following conclusions are drawn from this research.

1. Compared with the bare frame, the presence of infills significantly increased the stiffness and ultimate strength of the infilled frames. Even when gaps were present with the studied magnitude and location, the increases due to infill were pronounced.

2. Compared with the infilled frame with no gaps, the initial stiffness decreased when gaps were present. However, for a given gap location, the initial stiffness remained practically unchanged when the gap size increased from 7 to 12 mm. Furthermore, although the side gapped specimens showed a lower initial stiffness than the top gapped specimens with the same gap size, the variation was considered insignificant from a practical standpoint.

3. For the ultimate strength consideration, it seemed that gaps of 7 mm, regardless of the gap location, did not result in any significant reduction in the ultimate load when compared with the infilled frame without gaps. Gaps of 12 mm resulted in a more pronounced reduction (19% reduction on average) in the ultimate load and the reduction was more

significant for the top gap than for the side gap. When the loads at the three defined drift levels were considered, at the 1% drift level corresponding to post-disaster buildings, the presence of 7 mm or 12 mm gaps was found to cause reductions in the order of 20.0% and 47.5%, respectively; for the 2% and 2.5% drift levels corresponding to schools and all other buildings, no marked reductions caused by gaps were observed.

4. A preliminary assessment on the ductility showed that unreinforced masonry bounded by RC frames had improved ductility as specified in the NBCC 2010. The ductility ratio between the bare frame and the infilled frames obtained from this study indicated that the ductility of the masonry infilled RC frames was comparable to that of the RC bare frame.

5. For the stiffness prediction, CSA S304.1 grossly overestimated (about two times) the stiffness of the infilled frame with no gaps. It was found that reducing the calculated strut width by 60% for the infilled frame with no gaps resulted in an improved stiffness estimate, with a design-to-test stiffness ratio of about 1.5. For the gapped specimens, further reducing the strut width by 50% achieved the similar design-to-test stiffness ratio. On the other hand, the MSJC design stiffness agreed reasonably well with the experimental stiffness. Similarly, the reduction factor of 50% specified in MSJC 2011 yielded a reasonable design stiffness for the gapped specimens.

6. For the strength prediction, CSA S304.1 provided desired conservative estimates of the

ultimate strength for the infilled frames with no gaps or with 7 mm gaps; for the infilled frames with 12 mm gaps, application of a 50% reduction factor resulted in reasonable estimates. Similarly, the MSJC ultimate strength agreed reasonably well with the experimental ultimate strength. Applying the 50% reduction factor seemed to be harsh for the infilled frames with 7 mm gaps but worked well for the infilled frames with 12 mm gaps.

6.3 RECOMMENDATIONS FOR FURTHER RESEARCH

In summary, the results from this study suggest that in the design of masonry infilled frames, interfacial gaps of a certain magnitude may be accommodated in design. Figure 4.20 and 4.21 can be viewed as a preliminary guide. The reduction factor approach is simple and reasonable to use. However, due to the limited number of the specimens, the exact value of the magnitude of the gap and the reduction factor need more testing data to define. More specimens covering a wide range of gap magnitudes and locations need to be tested to provide an overall and in-depth understanding of the gap effect. For example, gap situations such as a full gap along the interface of the infill and the frame top beam and columns, side gap at only one side, a top gap plus one side gap, as well as gaps of other sizes (those place the frame in inelastic region) need more investigation. In addition, material and geometric properties, relative frame-to-infill stiffness ratios, and the effect of vertical load should also be included in any further study. For a long term objective, the infilled frame specimens subjected to cyclic loading should be tested to determine whether the findings from the static loading can be transferred to a cyclic loading situation.

REFERENCES

Abdul-Kadir, M.R. (1974). The structural behaviour of masonry infill panels in framed structures. Ph.D. Dissertation, University of Edinburgh, Edinburgh, England.

Al-Chaar, G. (2002). Evaluating strength and stiffness of unreinforced masonry infill structures. *Journal of Structural Engineering*, ASCE, 128(8):1055-1063.

Al-Chaar,G., Issa, M., and Sweeney, S. (2002). Behavior of masonry-infilled nonductile reinforced concrete frames. *Journal of Structural Engineering*, 128(8):1055-1063.

Angel, R. (1994). Behavior of reinforced concrete frames with masonry infill walls. Ph.D. Dissertation, the University of Illinois at Urbana-Champaign.

Asteris P. G., Antoniou S. T., Sophianopoulos D. S. Chrysostomou C. Z. (2011). Mathematical macromodeling of infilled frames: state of the art. *Journal of Structural Engineering*, 137 (12): 1508-1517

ASTM C143/C143M (2012). Standard test method for slump of hydraulic-cement concrete. ASTM International, West Conshohocken, PA.

ASTM C1314 (2014). Standard test methods for compressive strength of masonry prisms. ASTM International, West Conshohocken, PA.

ASTM C140/C140M (2014). Standard test methods for sampling and testing concrete masonry units and related units. ASTM International, West Conshohocken, PA.

ASTM C270 (2014). Standard specification for mortar for unit masonry. astm international, West Conshohocken, PA.

ASTM C39/C39M (2014). Standard test method for compressive strength of cylindrical concrete specimens. ASTM International, West Conshohocken, PA.

ASTM E8 (2008). Standard test methods for tension testing of metallic materials. ASTM International, West Conshohocken, PA.

CAN/CSA A165 (2004). CSA standards on concrete masonry units. Mississauga, ON, Canada: Canadian Standard Association.

CAN/CSA S304.1 (2004). Design of masonry structures. Mississauga, ON, Canada: Canadian Standard Association.

Carrillo, J., Conzalez, G., Rubiano, A. (2014). Displacement ductility of seismic design of RC wall for low-rise housing. *Latin American Journal of Solids and Structures*, 11:725-737.

Charleson, A. (2008). Reinforced concrete frame with brick masonry infill walls, digital image.<http://www.nexus.globalquakemodel.org/gem-building-taxonomy/overview/glossary/infilled-frame--lfinf >.

Comité Euro-International du Béton (CEB). (1996). RC frames under earthquake loading. State of the Art Rep., Tomas Telford Services, Ltd., London.

Dawe, J.L., and Seah, C.K. (1989). Behaviour of masonry infilled steel frames. *Canadian Journal of Civil Engineering*, 16(6): 865–876.

Drysdale, R.G., and Hamid, A.A. (2005). Masonry structures: behavior and design. Mississauga, Ontario: Canadian Masonry Design Centre.

El-Dakhakhni, W. W. (2002). Experimental and analytical seismic evaluation of concrete masonry-infilled steel frames retrofitted using GFRP laminates. Ph.D. Dissertation, Drexel University.

El-Dakhakhni, W., Elgaaly, M. and Hamid, A. (2003). Three-strut model for concrete masonry-infilled steel frames. *Journal of Structural Engineering*, 129(2), 177-185.

Federal Emergency Management Agency (FEMA). (2000). Prestandard and commentary for the seismic rehabilitation of buildings, FEMA-356, Building Seismic Safety Council, Washington, D.C.

Flanagan, R. D., & Bennett, R. M. (1999). In-plane behavior of structural clay tile infilled frames. *Journal of Structural Engineering*, ASCE, 125(6):590-599.

Galanti, F.M.B., Scarpas, A. and Vrouwenvleder, A.C.W.M. (1998). Calibration of a capacity design procedure for infilled reinforced concrete frames, Eleventh European Conference on Earthquake Engineering-Balkema, Rotterdam, 1-10.

Hendry, A. (1981). Structural brickwork. Macmillan, London.

Holmes M. (1961). Steel frames with brickwork and concrete infilling. *Proceedings of the Institution of Civil Engineers*, 19: 473-478.

Liauw, T.C. and Kwan, K.H. (1983). Plastic theory of infilled frames with finite interface shear strength. *Proceedings of the Institution of Civil Engineers*, 78, 707-723.

Liu, Y. and Soon, S. 2012. Experimental study of concrete masonry infills bounded by steel frames. *Canadian Journal of Civil Engineering*, 39: 180–190.

Mainstone, R. J. (1971). On the stiffness and strengths of infilled frames. *Proceedings of the Institute of Civil Engineers*, Suppl. (4):57–90.

Maleki, M., Hamid, A.A., El-Damatty, A.A. and Drysdale, R.G. (2007) Behavior of partially grouted reinforced concrete masonry panels under in-plane diagonal loading. *Proceedings of the 10th North American Masonry Conference*, pp. 1039-1050.

Masonry Standard Joint Committee (2011). Building code requirements for masonry structures. ACI 530/ASCE 5/TMS 402. American Concrete Institute, the American Society of Civil Engineers and the Masonry Society. USA.

Manesh, P.B. (2013). Experimental study of masonry-infilled steel frames subjected to combined axial and in-plane lateral loading. MASc thesis, Dalhousie University, Halifax, Canada.

Mehrabi, A. B., Shing, P. B., Schuller, M. P., and Noland, J. L. (1996). Experimental evaluation of masonry-infilled RC frames. *Journal of Structural Engineering*, ASCE, 122(3):228-237.

Moghaddam, H., & Dowling, P. (1988). Earthquake resistant design of brick infilled frames. Brick and Block Masonry (8th IBMAC) London, Elsevier Applied Science, 2:774-784.

Mosalam, K. H., White, R. N., and Gergely, P. (1997). Static response of infilled frames using quasi-static experimentation. *Journal of Structural Engineering*, ASCE, 123(11)1462-1469.

Nazief, M.A. (2014). Finite element characterization of the behaviour of masonry infill shear walls with and without openings. Ph.D. dissertation, University of Alberta, Edmonton, Canada.

NBCC (2010). National building code of Canada. Institute for Research in Construction, NRCC, Ottawa, Ontario.

Ng'andu, B.M. (2006). Bracing steel frames with calcium silicate element walls. Ph.D. dissertation, Eindhoven University of Technology, the Netherlands.

Paulay, T., & Priestley, M. J. N. (1992). Seismic design of reinforced concrete and masonry buildings, Wiley New York.

Polyakov, S. V. (1956). Masonry in framed buildings (An investigation into the strength and stiffness of masonry infilling). Gosudarstvennoe izdatel'stvo Literatury po stroitel'stvu iarkhitekture, Moscow. (English translation by G. L. Cairns, National Lending Library for Science and Technology, Boston, Yorkshire, England, 1963).

Riddington, J. R. (1984). The influence of initial gaps on infilled frame behavior. *Proceedings of the Institute of Civil Engineers*, 77(3):295-310.

Rosenblueth. E. (1980). Design of earthquake resistant structures. Pentech Press Limited: 195-222.

Stafford-Smith, B., and Carter, C. (1969). A method of analysis for infilled frames. *Proceedings of the Institution of Civil Engineers*, 44(1):31-48.

Stafford-Smith, B., and Coull, A. (1991). Tall building structures: analysis and design, Wiley-Interscience.

Salonikios, T., Kappos, A., Tegos, L., Penelis, G. (2000). Cyclic load behaviour of low-slenderness reinforced concrete walls: failure modes, strength and deformation analysis, and design implications. *ACI Structural Journal*, 97(1):132-142.

Seah, C.K. (1998). A university approach for the analysis and design of masonry infilled frames structures. Ph.D. Dissertation, University of New Brunswick.

Soon, S. (2011). In-plane behavior and capacity of concrete masonry infills bounded by steel frames. MASc thesis, Dalhousie University, Halifax, Canada.

Tawfik, A.S., Badr, M.R., Elzanaty, A. (2014). Behavior and ductility of high strength reinforced concrete frames. *HBRC Journal*, 10, 215–221.

Wood, R.H. (1978). Plasticity, composite action and collapse design of unreinforced shear wall panels in frames. *Proceedings of the Institution of Civil Engineers*, 65(2):381-411.

World house encyclopedia, Steel moment resisting frame with brick masonry partitions, digital image. < http://db.world-housing.net/building/95 >.

Yong, T.C. (1984). Shear strength of masonry infilled panel in steel frames. MSc thesis, University of New Brunswick, Fredericton, Canada.

APPENDIX A DESIGN STIFFNESS AND STRENGTH CALCULATIONS

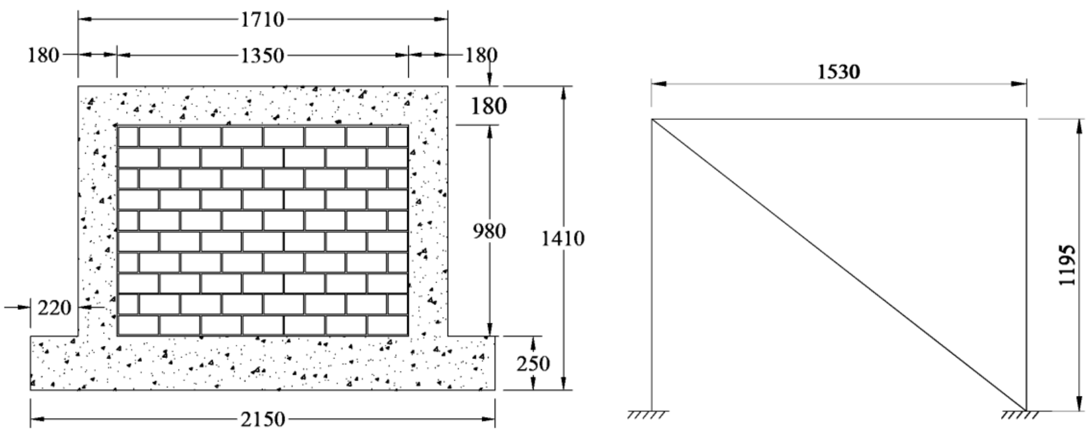

(a) (b)

Figure A.1 (a) Infilled frame specimen; (b) SAP2000 model

<u>**Specimen IFNG**</u>

Frame Properties:

E_f = 28424 MPa f'_c = 42.3 MPa $I_b = I_c = 8.748\times10^7$ mm^4

h'= 1195 mm l' = 1530 mm

Infill Properties:

E_m = 14195 MPa f'_m= 16.7 MPa

h = 980 mm l = 1350 mm t = 90 mm t_f = 17 mm t_e = 34 mm

Specimen IFSG7

Frame Properties:

E_f = 29259 MPa f'_c = 45.3 MPa $I_b = I_c = 8.748 \times 10^7$ mm^4

h'= 1195 mm l' = 1530 mm

Infill Properties:

E_m = 14535 MPa f'_m= 17.1 MPa

h = 980 mm l = 1350 mm t = 90 mm t_f = 17 mm t_e = 34 mm

CSA S304.1

The specimen IFNG was taken as the CSA calculation example.

Stiffness calculation

The effective width based on CSA S304.1 was used to calculate the stiffness. The calculation was as follows:

$$w = \frac{1}{2}\sqrt{{\alpha_h}^2 + {\alpha_L}^2} = \frac{1}{2}\sqrt{599^2 + 1299^2} = 715\,\text{mm}$$

where,

$$\alpha_h = \frac{\pi}{2}\sqrt[4]{\frac{4E_f I_c h}{E_m t_e \sin 2\theta}} = \frac{3.14}{2}\sqrt[4]{\frac{4(28424)(87480000)(980)}{(14195)(34)\sin(2(0.628))}} = 599\,\text{mm}$$

$$\alpha_L = \pi\sqrt[4]{\frac{4E_f I_b l}{E_m t_e \sin 2\theta}} = 3.14\sqrt[4]{\frac{4(28424)(87480000)(1350)}{(14195)(34)\sin(2(0.628))}} = 1299\,\text{mm}$$

where,

$$\theta = \tan^{-1}\frac{h}{l} = \tan^{-1}\frac{980}{1350} = 0.628\,\text{rad}$$

$$l_d = \sqrt{h^2 + l^2} = \sqrt{980^2 + 1350^2} = 1668\,\text{mm}$$

CSA S304.1 cl. 7.13.3.3 states that the effective width shall not exceed 0.25 of the diagonal length of the infill, thus the design width of the strut is determined as:

$$w = \frac{l_d}{4} = \frac{1668}{4} = 417\,\text{mm}$$

A SAP2000 model was created with the material and geometric properties. The design width of the strut was adopted as the width of the bracing. 100 kN was placed at the top of the frame. A linear static analysis was performed and the lateral displacement was obtained as 1.22 mm, as illustrated in Figure A.2.

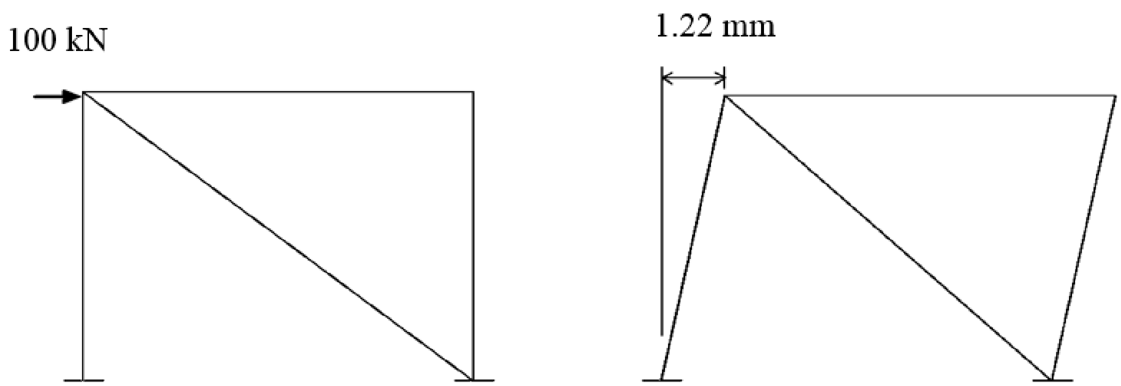

Figure A.2 Illustration of the braced frame

Thus the stiffness was:

$$K = \frac{100}{1.22} = 82.0\,\text{kN/mm}$$

Strength calculations

1. Diagonal cracking strength

$$P_{cra} = \phi_m (v_m b_w d_v + 0.25 P_d)\gamma_g = 1.0(1.14(90)(1080) + 0.25(0))(0.38) = 42.0\,\text{kN}$$

where,

ϕ_m = 1.0 (resistance factor set to unity to compare with the raw experimental data)

$$v_m = 0.16(2 - \frac{M_f}{V_f d_v})\sqrt{f'_m} = 0.16(2 - 0.25)\sqrt{16.7} = 1.144$$

$\frac{M_f}{V_f d_v} = 0.25$ (taken as the minimum value of 0.25 though M_f is zero)

$b_w = t = 90\,\text{mm}$

$d_v = 0.8l = 0.8(1350) = 1080\,\text{mm}$

$P_d = 0$ (as self-weight is negligible)

$\gamma_g = t_e/t = 0.38$

2. Shear sliding strength

$$V_r = 0.16\phi_m \sqrt{f'_m} A_{uc} + \phi_m \mu \mathrm{P}_1 = 0.16(1.0)(\sqrt{16.7})(36720) + (1.0)(1.0)(0.726 V_\mathrm{r}) = 87.6\text{ KN}$$

where,

$A_{uc} = 0.8 l t_e = 0.8(1350)(34) = 36720\,\text{mm}^2$

$\mu = 1.0$ (for masonry to masonry sliding friction)

$P_1 = 0.726 V_r$ (taken as the vertical component of the diagonal compression force)

3. Corner crushing strength

For the compressive capacity (corner crushing strength in this case) of the diagonal strut, from CSA S304.1 (7.13.3.4), the effective strut length for slenderness effects is l_d-w:

$$l_d - w = 1668 - 417 = 1251 \text{ mm}$$

$$\frac{k(l_d - w)}{t} = \frac{0.9(1251)}{90} = 12.5 < 30 \text{ OK}$$

$$\mathrm{P_r} = \phi_m \chi (0.85 f'_m) b(2t_f - r) = 1.0(0.5)(0.85 \times 16.7)(417)(2 \times 17 - 6) = 82.9 \text{ kN}$$

where,

$\chi = 0.5$ (CSA S304.1 cl 10.2.6)

k = 0.9 (effective length factor, CSA S304.1 Annex B)

$b = w = 417$ mm

$$r = (\frac{t}{2} + e) - \frac{1}{2}\sqrt{t^2 + 4te + 4e^2 - 16et_f} = (\frac{90}{2} + 9) - \frac{1}{2}\sqrt{90^2 + 4(90)(9) + 4(9)^2 - 16(9)(17)} = 6$$

where, $e = 0.1t = 0.1 \times 90 = 9$ mm (taken as the minimum value of $0.1t$ as the initial eccentricity)

$$P_{cr} = \frac{\pi^2 \phi_e (EI)_{eff}}{(kh)^2 (1 + 0.5\beta_d)} = \frac{3.14^2 (1.0)(1.09 \times 10^{11})}{(0.9 \times 1251)^2 (1 + 0.5 \times 0)} = 84.9 \text{ kN}$$

where,

$\phi_e = 1.0$ (resistance factor set to unity to compare with raw data)

$\beta_d = 0$ (for temporary loading)

$(EI)_{eff} = 0.4E_m I_o = 0.4 \times 24195 \times 1.92 \times 10^7 = 1.09 \times 10^{11}$ mm^4

h is the effective length of the strut, determined as l_d-w.

$I_0 = \dfrac{(90^3 - (90 - 2\times17)^3)(417)}{12} = 1.92\times10^7$ mm^4 (moment of inertia of the uncracked effective cross-sectional area)

$$e' = \frac{1}{1-\left(\dfrac{P_r}{P_{cr}}\right)}e = \frac{1}{\left(1-\dfrac{82.9}{84.9}\right)}(9) = 9.98\,\text{mm}$$

Once the first iteration e' is obtained, it can replace the previous e to reiterate the results. An iteration process is carried out between e and e' until they converge. The final P_r and P_{cr} results are 81.2 kN and 84.9 kN, respectively. Using these values,

$$P_{uil} = \frac{l}{l_d}P_r = \frac{1350}{1668}(81.2) = 65.7\,\text{kN}$$

MSJC 2011

Since shear sliding failure only occurred in specimens with side gaps (IFSG7 and IFSG12), here specimen IFSG7 was taken as the MSJC calculation example. The 50% reduction factor was applied to the infill stiffness and strength.

Stiffness calculation

The width of the strut is calculated as following:

$$w = \frac{0.3}{\lambda\cos\theta} = \frac{0.3}{(0.00262)\cos(0.628)} = 142\,\text{mm}$$

where,

$$\lambda = \sqrt[4]{\frac{E_m t \sin 2\theta}{4E_f I h}} = \sqrt[4]{\frac{(14535)(34)\sin 2(0.628)}{4(29259)(87480000)(980)}} = 0.00262$$

As the strut is in compression. Reducing the strut width to half will yield a half discounted stiffness of the infill. A linear analysis of the braced frame with the MSJC design strut width showed that the infilled frame stiffness was 41.8 kN/mm.

Strength calculation

MSJC 2011 provided equations for the determination of the infill strength based on three states, namely, the corner crushing failure, shear sliding failure and 25 mm lateral displacement.

Corner crushing failure

$$V_r = (6.0in)t_{\mathrm{e}} f'_m = (6 \times 25.4)(34)(17.1) = 88.6\,\mathrm{kN}$$

$$P_{ult} = 0.5V_r = 0.5(88.6) = 44.3\,\mathrm{kN}$$

Shear sliding failure

$$V_r = \frac{V_n}{1.5}$$

where,

$$V_n = \min \begin{cases} 3.8A_{nv}\sqrt{f'_m} \\ 300A_{nv} \\ or \\ 56A_{nv} + 0.45N_u \quad \text{if not fully grouted} \\ 90A_{nv} + 0.45N_u \quad \text{if fully grouted} \end{cases}$$

and where,

$\sqrt{f'_m} = \sqrt{17.1MPa} = \sqrt{2480\,psi}$

$N_u = 0.726V_n$ (compressive force acting normal to shear surface, taken as the vertical component of the diagonal compression)

$A_{nv} = 0.8lt_e = 0.8(1350)(34) = 36720\,\text{mm}^4 = 56.9\ \text{in}^2$

Therefore,

$V_n = 56(56.9) + 0.45(0.726)(V_v)$

$V_n = 4733\,\text{lb} = 21.1\ \text{kN}$

$V_r = \dfrac{V_n}{1.5} = \dfrac{21.1}{1.5} = 14.1\,\text{kN}$

25 mm lateral displacement

With a horizontal force of 1100 kN, a lateral displacement of 25 mm was achieved of the braced frame in SAP2000. The compression force in the diagonal strut was obtained as 686 kN, thus the horizontal share of the compression force was 555 KN. The design strength was determined to be 277.5 kN after the application of 50% reduction factor.

APPENDIX B FRAME ELASTIC DISPLACEMENT CALCULATIONS

The elastic displacement was calculated based on the assumptions that the tensile resultant was only taken by the reinforcing steel, A_s; the compressive resultant was shared by the reinforcing steel A'_s and the hatched concrete, as shown in Figure B.1.

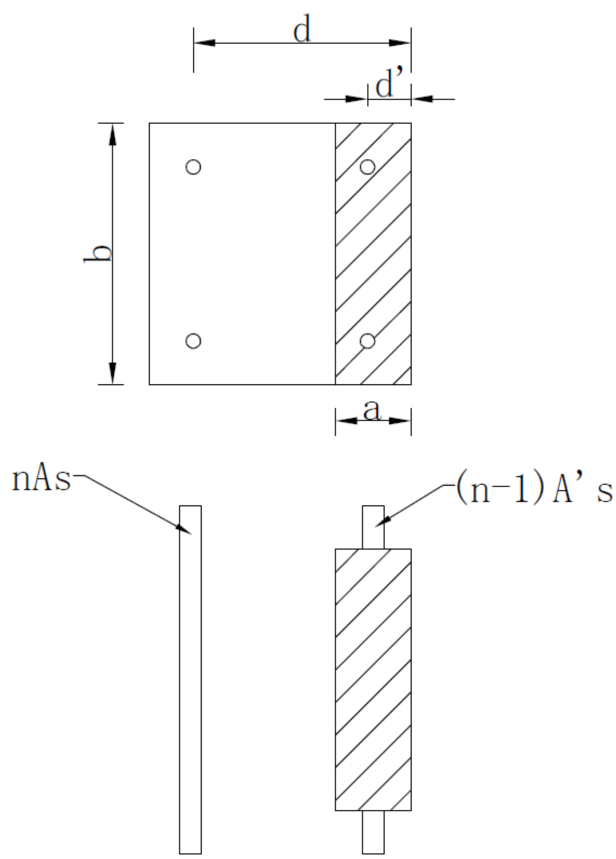

Figure B.1 Transformed cross-section of the column

Known properties of the section:

$b = 180\,\mathrm{mm}$ $\qquad d' = 40\,\mathrm{mm}$ $\qquad d = 140\,\mathrm{mm}$

$n = \dfrac{E_s}{E_c} = \dfrac{247357}{28424} = 8.7$ $\qquad A'_s = A_s = 200\,\mathrm{mm}^2$

The three parts, namely, the tensile steel, the compressive steel and the effective compressive concrete satisfy the following relationship with respect to the neutral axis:

$$ab(\frac{a}{2}) + (n-1)A'_s(a-d') = nA_s(d-a)$$

$$a(180)(\frac{a}{2}) + (8.7-1)(200)(a-40) = 8.7(200)(140-a)$$

Thus the depth of the compressive concrete, a, is calculated as 42.8 mm

The moment of inertia of the cracked section was calculated from the transformed section, as shown in Figure B.1. The process was presented as follows,

$$I_{cr} = \frac{ba^3}{3} + nA_s(d-a)^2 + (n-1)A'_s(a-d')^2 = 2.12\times10^7\,\mathrm{mm}^4$$

The moment of inertia of the uncracked section taking into account the reinforcement was calculated as follows,

$$I_g = \frac{b^4}{12} + (n-1)A_s(\frac{b}{2}-d') + (n-1)A'_s(\frac{b}{2}-d') = 9.52\,\mathrm{mm}^4$$

Through an elastic analysis of the critical section of the column at the loaded side, the following equation can be made:

$$n(\frac{My}{I_{cr}} + \frac{P}{A_{cr}}) = F_y = 446\,\mathrm{MPa}$$

where,

$$A_{cr} = ab + nA_s + (n-1)A'_s = 10984\,\mathrm{mm}^2$$

$y = d - a = 140 - 42.8 = 97.2\,\text{mm}$

M and P satisfy the following relationship from an analysis of the bare frame in SAP2000, where F is an arbitrary load.

$M = 351F$ (kN·mm)

$P = 0.32F$ (kN)

Thus the F can be determined as 31.3 kN. This is the load that make the reinforcing steel in the column at the tensile side start to yield. The lateral displacement at this load was obtained as 6.3 mm from the bare frame analysis in SAP2000. The displacement at this load from the test of the bare frame was 7.6 mm. Therefore the elastic displacement of the frame can be determined as the average of these two values, i.e., 7 mm.